

CZECH TECHNICAL UNIVERSITY IN PRAGUE
FACULTY OF ELECTRICAL ENGINEERING



BACHELOR THESIS

2022

IBRAHIMOV RUFAT



CZECH TECHNICAL UNIVERSITY IN PRAGUE

FACULTY OF ELECTRICAL ENGINEERING
DEPARTMENT OF PHYSICS

BACHELOR WORK:
"CHARACTERIZATION OF OPTICAL COLOR CENTERS IN DIAMONDS"

Rufat Ibrahimov
Prague, May 2022

Bachelor program: Electrical engineering and computer science
Branch of study: Electrical engineering
Academic year: 2021/2022

Supervisor of the work:

Ing. Stepan Potocky, Ph.D.

I. Personal and study detailsStudent's name: **Ibrahimov Rufat**Personal ID number: **485680**Faculty / Institute: **Faculty of Electrical Engineering**Department / Institute: **Department of Physics**Study program: **Electrical Engineering and Computer Science****II. Bachelor's thesis details**

Bachelor's thesis title in English:

Interaction of optically active thin diamond films with biomolecules

Bachelor's thesis title in Czech:

Interakce opticky aktivních tenkých diamantových vrstev s biomolekulami

Guidelines:

1. Get acquainted with the current state of the optical centers based on silicon vacancies centers in diamond – fabrication of thin-film and the influence of molecular adsorption on the luminescence properties of the optical centers.
2. Examine and analyze strategies for growth of ultrathin diamond layers, incorporation of Si into diamond during the chemical vapor deposition process, diamond surface modifications, and adsorption of molecules using the literature.
3. Fabricate a set of thin diamond films with Si-V optical centers, bond the selected molecules, and examine their influence on the photoluminescence behavior.
4. Compare the results based on film thickness, surface termination, and bonded molecule with the outlook for biosensing.

Bibliography / sources:

- [1] S. Potocky et al., Physica Status Solidi (A), 2015, 251, 2580. DOI 10.1002/pssb.201552222
- [2] S. Stehlík et al., ACS Appl. Mater. Interfaces, 2017, 9, 38842. DOI I: 10.1021/acsami.7b14436
- [3] H.-C. Chang et al., Fluorescent Nanodiamonds. John Wiley & Sons, Ltd, 2018. DOI 10.1002/9781119477099
- [4] S. Stehlík et al., Micromachines, 2018, 9, 281. DOI 10.3390/mi9060281
- [5] A. Artemenko et al., Diamond and & Related Materials, 2019, 100, 107562. DOI 10.1016/j.diamond.2019.107562
- [6] J.N. Becker et al., Semiconductors and Semimetals, 2020, 103, 201. DOI 10.1016/bs.semsem.2020.04.001
- [7] B. Rezek et al., Physica Status Solidi (A), 2021, 218, 2000558. DOI 10.1002/pssa.202000558

Name and workplace of bachelor's thesis supervisor:

Ing. Štěpán Potocký, Ph.D. Department of Physics FEE

Name and workplace of second bachelor's thesis supervisor or consultant:

Date of bachelor's thesis assignment: **09.02.2022** Deadline for bachelor thesis submission: **15.08.2022**Assignment valid until: **30.09.2023**

Ing. Štěpán Potocký, Ph.D.
Supervisor's signatureprof. Ing. Ondřej Jiříček, CSc.
Head of department's signatureprof. Mgr. Petr Páta, Ph.D.
Dean's signature**III. Assignment receipt**

The student acknowledges that the bachelor's thesis is an individual work. The student must produce his thesis without the assistance of others, with the exception of provided consultations. Within the bachelor's thesis, the author must state the names of consultants and include a list of references.

Date of assignment receipt

Student's signature

Declaration

2

I hereby declare I have written this bachelor thesis independently assuming that the results of the thesis can also be used at the discretion of the supervisor of my bachelor work as its co-author and quoted all the sources of information used in accordance with methodological instructions on ethical principles for writing an academic thesis. Moreover, I state that this thesis has neither been submitted nor accepted for any other degree. I also agree with the potential publication of the results of the thesis or of its substantial part, provided I will be listed as the co-author.

In Prague, date: _____

Rufat Ibrahimov

Abstract

3

When two carbon atoms in the diamond lattice are replaced with one silicon atom, the defects in diamonds, known as Si-V color centers, are formed. Si-V vacancies have a characteristic peak at 738-739[nm] and show great potential in biochemical and quantum processing application. In this work we prepare multiple silicon samples and oxygenate half of them, nucleate them with a specially prepared O-DnD 520/30 (detonation nano-diamond) solution of 2mg/ml. Such nucleated samples of 2-4[nm] thick layer would have an optimal density of the nucleated surface grains in the power of 10^{11} [cm^{-2}], while conventional have 10^5 [cm^{-2}] on average. We conduct SEM (Scanning electron microscopy) analysis on them and observe density of the nucleated surface in three spots of 200x200[nm^2] scale in [cm^{-2}] units from each scan. The NCD (nano-crystalline diamond) preparation is done in the ellipsoidal resonator CVD chamber with addition of H₂ and CH₄ (95/5% ratio respectfully) and pure silicon for creation of the Si-V centers and the goal of achieving thin NCD surface on top of the Si substrates of less than 50[nm]. In order to research potential biochemical application, chemicals BSA (Bovine Serum Albumin) and FBS (Fetal Bovine Serum) are drop-cast on top of the thin NCD layer. After observing their electronic and vibrational characteristics through spectroscopy(Raman, AFM, PL) we observe impact of chemicals on their surface regarding the Si-V vacancies.

Keywords: Nano-crystalline diamond, photoluminescence, atomic force microscopy, silicon vacancies, Si-V peak, color centers, scanning electron microscopy, detonation nano-diamond, oxygen plasma, chemical vapor deposition, bovine serum albumin, fetal bovine serum, nucleation stages, nucleation density, Si and O-Si groups.

Acknowledgements

4

First and foremost, I would like to greatly thank my supervisor, Ing. Stepan Potocky for providing me with useful information and especially, for always explaining every little detail of the work that was or was not clear to me, as many times as was necessary and most importantly his patience towards me and my attitude. My gratitude also goes towards Bohuslav Rezek, Jaroslav Kulicek, Jitka Libertinova and Egor Ukraintsev for their assistance in training in the equipment operation or providing additional guidance and insight towards the work refinement and completion.

My family and close ones were very supportive of me at every step of writing this work and, I want to give my warm thanks towards every one of them, especially my parents, who gave me with this opportunity. And finally, I am thankful for the small group of friends that made years in the university more entertaining and productive.

List of tables and formulae

5

Table 1: Features of three electron guns.....	23
Table 2: Density of the grains in O-Si (oxygenated prior to seeding) and Si samples in 3 nucleation stages from the minimal grain size of 2[nm] to 7[nm] in diameter with a 1[nm] step and also 10[nm] in diameter (pxls ² is pixels).....	30
Formula 1.....	28
Formula 2.....	29

List of figures

6

Figure 1.1: Oxygen plasma inside the chamber.....	16
Figure 1.2: Ultrasonic probe “Dr.Heilsher UP300S”.....	18
Figure 1.3:Microcentrifuge “Benchmark MC-12”	18
Figure 2.1: Schematic drawing of the electron and x-ray optics of a combined SEM-EPMA.....	20
Figure 2.2: Process of incident electrons contacting the sample’s surface.....	21
Figure 2.3: SEM microscope schematic.....	24
Figure 2.4: Scanning electron microscope MAIA3 (TESCAN)	24
Figure 2.5: Seeded Si samples place on the SEM wafer.....	25
Figure 2.6: SEM scan of O-Si nucleated samples of 1 st , 2 nd , and 3 rd stage (left to right respectively).....	27
Figure 2.7: SEM scan of Si nucleated samples of 1 st , 2 nd , and 3 rd stage (left to right respectively).....	27
Figure 2.8: “Analyze particles” option.....	28
Figure 2.9: “Threshold” option to outline grains in imageJ.....	29
Figure 2.10: a - SEM image of 3 rd stage Si “fine” nucleation; b - 8-bit scale of the said image after changing the contrast by threshold command; c - the highlighted grains on the scan after setting the maximal pixel size; all the images are in a 200x200[nm] area.....	30
Figure 2.11: Minimal grain size conversion from table 2 from nm to nm ² and pxls and from newfound pxls to pxls ² with approximation to integer.....	31
Figure 2.12: Density comparison for minimal grain diameter of 4[nm] at different nucleation stages for Si and O-Si.....	32
Figure 2.13: Density curves of 3 nucleation stages for Si and O-Si samples, that show changes in density in regard to the minimal grain diameter.....	32
Figure 3.1: Energy/gasses involved in the CVD.....	34
Figure 3.2: “Bell-jar” ellipsoidal CVD resonator.....	34
Figure 3.3: Schematic of an ellipsoidal CVD chamber, where MW is the microwave oven and F1/F2 are the focal points.....	34
Figure 3.4: Gas exhaust system.....	35
Figure 3.5: Substrate holder with the nucleated silicon samples in the middle.....	35

List of figures

7

Figure 4.1: Diagram showing influence on the energy levels by elastic (Rayleigh) and inelastic (Raman or Stokes and Anti-Stokes) spectroscopies].....	38
Figure 4.2: AFM measurement example. Laser light falls on the pin, which is affected by the repulsive force and the light sends data to the detector.....	41
Figure 4.3: Optical confocal Raman microscope.....	42
Figure 4.4: Optical confocal Raman microscope structure.....	42
Figure 4.5: AFM microscope Dimension Icon Bruke.....	44
Figure 4.6: PL Si-V peak of a thick (>150 nm) NCD deposited sample (Low peak) and the influence of the laser (High peak).....	45
Figure 4.7: Raman spectra of a thick (>150nm) NCD sample ($\lambda_{exc} = 532\text{nm}$).....	46
Figure 4.8: PL intensity of the NCD deposited thick (>150nm) sample over the λ_{exc} of the laser showing Si-V and laser interference peaks from 400nm to 700nm with a 5nm step.....	47
Figure 4.9: PL spectra of 16[nm] H-term(hydrogenated) NCD layer under four different integration times.....	48
Figure 4.10: Raw tilted 3D map of the 1 st stage “fine” nucleated and later deposited for 15 minutes NCD surface on top of silicon topography. a) view from the top; b) view from the side.....	50
Figure 4.11: 5 line scans of filtered topography of the 1st stage “fine” nucleation deposited NCD surface (15 minutes in CVD) on top of silicon, indicated by respective numbers.....	50
Figure 4.12: Filtered AFM topography of the 1st stage “fine” nucleation deposited NCD surface (15 minutes in CVD) on top of silicon, original and masked.....	51
Figure 4.13: Filtered & leveled AFM of deposited Si substrate samples of 3 “fine” nucleation stages: a) 1st stage 15[min] CVD; b) 2nd stage 10[min] CVD; c) 3rd stage 5[min] CVD.....	52
Figure 4.14: AFM topography of nucleated “fine” method samples of 2 nd and 3 rd stages with their respective line scans a) 2 nd stage nucleation topography/line scan; b) 3 rd stage nucleation topography/line scan.....	53
Figure 4.15: PL analysis Si-V peak spectra comparison of the Si and O-Si(Oxygenated during the nucleation stage) groups of the 92[nm] NCD layered samples.....	53

List of figures

8

Figure 5.1: Figure 5.1: On the left: Raman spectrum comparison with an NCD peak of O-term NCD(top) and H-term NCD(bottom) of NCD “fine” thin layer samples deposited for 5, 10 and 15 minutes and pure silicon, with NCD peak at 1339 cm^{-1} ; On the right: PL of the NCD surface with an Si-V peak at 738 nm of thin layer samples deposited for 5(bottom), 10(middle) and 15 minutes(top) with O-term and H-term NCD comparison on each.....	56
Figure 5.2: PL spectrum of the drop-cast NCD samples of 25[nm], 32[nm] and 92[nm] with BSA on top(O-term).....	57
Figure 5.3: PL spectrum of the drop-cast NCD samples of 25[nm], 32[nm] and 92[nm] with BSA on top (H-term)]	57
Figure 5.4: PL spectra of pure silicon with two signals: from the Si surface and from BSA drop-cast on top of it.....	58
Figure 5.5: PL spectra of 16[nm] thick “fine” NCD layer at 50% laser power(left) and 15% laser power(right) with signals of pure Si(orange); NCD(blue); washed BSA drop-cast on NCD(yellow) and washed FBS drop-cast on NCD(grey)	59
Figure 5.6: PL spectra of 16[nm] thick “fine” H-term(right) and O-term(left) NCD layers with signals of FBS on pure Si(yellow); NCD(blue); BSA drop-cast on NCD(orange) and FBS drop-cast on NCD(blue)	59

List of acronyms and abbreviations

9

- CVD – Chemical vapor deposition
NCD – Nanocrystalline diamond
Si-V – Silicon vacancy
Ni-V – nitrogen vacancy
DnD – Detonation nano diamonds
PL – Photoluminescence
MW – Microwave
ZPL – Zero-phonon line
MWPCVD - microwave plasma-assisted chemical vapor deposition
H-DND - hydrogen-terminated DND
ZP – zeta-potential
RMS – root-mean square
FTIR - Fourier transform infrared spectroscopy
PLEN – part below the substrate holder
FZU – University of Physics
Rpm – Rotations per minute
US – Ultrasound/Ultrasonic
DI – Deionized
SCCM - Standard cubic cm/min
PLQY - PL quantum yield
BSE – backscattered electrons
SEM – scanning electron microscopy
SEM-EPMA – Scanning electron microscope-mounted electron probe x-ray microanalysis
EDS – Energy-dispersive X-ray spectroscopy
WD – Working distance
Pxls – Pixels
SCCM – Standard Cubic Cm per Minute
SPM – Scanning Probe Microscopy
IR – Infrared
NIR – Near-IR
PLQY – Photoluminescence quantum yield
STM – Scanning tunnelling microscopy
CCD – Charged couple device

Contents

10

Abstract.....	3
Acknowledgements.....	4
List of tables and formulae.....	5
List of figures.....	6
List of acronyms and abbreviations.....	9
Contents.....	10
Introduction.....	12
Chapter 1 – Nucleation.....	15
“Standard” vs “fine” nucleation method and first steps...15	
Oxygen plasma.....	16
Preparation of the DnD solution.....	17
Nucleation.....	18
Chapter 2 – SEM.....	20
What is SEM.....	20
How SEM works.....	21
SEM microscope structure.....	23
Measurement steps.....	25
Experimental section.....	26
Results.....	31
Chapter 3 – CVD.....	33
What is CVD and how does it work.....	33
State of the art/equipment.....	34
Experimental section.....	36
Chapter 4 – Raman, AFM, PL.....	38
What is Raman spectroscopy.....	38
What is PL spectroscopy	39
What is AFM.....	40
State of the art/equipment.....	42
Experimental part.....	44

Contents

11

Conclusion.....	55
Summary of thesis and fulfillment of the targets.....	55
Further extensibility and recommendations.....	60
Bibliography.....	61

Introduction

12

In diamonds there exists a defect, that appears in the material by artificial means, through CVD chamber or silicon doping. Although, its occurrences have been reported in natural gem-quality colorless diamonds, specifically in the work from 2008^[1] for the first time. These defects are called “color centers” and they represent trapped electrons/holes in transparent materials. When material has this defect it loses own transparency and experiences changes in coloration, hence the name “color centers”. They are either formed by impurity atoms or shift in the structure of the diamond lattice and for us, and for this work, the latter is of a great interest. These defects have shown excellent potential for application in various fields, such as photonics and biology^[2]. There is numerous color center, such as F-centers or M-centers, but the most extensively studied are the nitrogen-vacancy centers or N-V. Additionally, in the years at least since 2017, there was a growing interest in silicon vacancies or Si-V centers, as in comparison to N-V centers, they have a wide emission spectrum at around 22-26°C. Si-V centers have an advantage in their narrow zero-phonon line (ZPL) at the same temperature. On the spectrum this characteristic is shown as a peak at 738-739[nm] wavelength, and about 70% of ZPL reside there.^[2] Interest to them rose because of their optical properties, that can be observed through the PL (photoluminescence) spectroscopy and their application to the biosensors has some potential as well. It was discovered that Si-V centers are sensitive to surface chemistry of nanodiamond, but it is not yet clear how deeply can the surface chemical groups, such as BSA (Bovine Serum Albumin) or FBS (Fetal Bovine Serum), change the Si-V PL peak. In order for the biosensor to react optimally when the environment surrounding it experiences changes, high concentration of Si-V centers on the NCD (Nano-crystalline diamond) surface is required.^[2] And in order for this concentration to take place, the NCD layer thickness should be as thin as possible. This concept has other advantages, for example pulling the Si-V centers closer to the surface of the NCD film. However, measurements from this work show that thicker samples (~92nm) have higher photoluminescence peak intensity that is characteristic to Si-V, than those with a thinner layer(~32nm). For this comparison, silicon samples (which provide great substrates for such case, as they are relatively cheap and reliable) with a thicker NCD layer deposited on top, were created, in a less complicated way. The only difference between the two groups is a nucleation stage, primarily creation of DnD (detonation nanodiamond) solution from the eponymous powder. There are different methods of creating NCD with Si-V centers, such as annealing, ion implantation or electron bombardment^[3] and many others, but the most suitable method for this goal that we will utilize is the chemical vapor deposition (CVD) process. In addition to this, the preparation of diamond color centers by CVD method has many positive features. The size of diamond crystal and the volume in diamond color center can be well controlled throughout time for different reasons, “the substrate selection of diamond growth is diversified, and specific impurity elements can be doped”.^[4]

Nucleation stage is really important for the NCD creation. Carbon atoms don't react with silicon atoms, so in the CVD chamber no NCD layer would appear as a result. For thinner layer

and presence of Si-V color centers in NCD, a special method of nucleation should be considered. It is usually referred to as “fine” nucleation method and it utilizes a thorough approach to the creation of the DnD solution. DnD powder undergoes hydrogenation and oxidization, losing its initial mass and after mixing with water it is declustered and centrifuged in a microcentrifuge 3 times, in order to absolve the mud and separate it from pure O-DND 520/30 solution. The pure DnD solution serves as a great source of nucleation, as diamond grains appear smaller and closer to each other, creating high density and resulting in a better CVD process and thinner NCD layer as a result. There are 3 stages that this DnD solution undergoes, increasing by one each time nucleation the silicon samples occur. The 1st and 4th (and further) stages are presumed to be the worst with heavily aggregated diamond grains and stages 2 and 3 are the most ideal, creating the highest density theoretically. Performing SEM measurements on the samples displays good results, of 1st stage of nucleation being the least dense out of all three and 2nd and 3rd stages displaying high density of $10^{11} [\text{cm}^{-2}]$ and theoretically even $10^{12} [\text{cm}^{-2}]$ if the average size of the grains was as small as 1[nm], however this is not close to the stable and consistent $10^{12} [\text{cm}^{-2}]$ order of density achieved in the “Ultrathin Nanocrystalline Diamond Films with Silicon Vacancy Color Centers via Seeding by 2 nm Detonation Nanodiamonds” article by Stepan Stehlík.^[2] O-DnD 520/30 solution was distributed on the samples in a 2mg/ml ratio. The densities were estimated from the SEM analysis scans using imageJ, and the highest recorded density of the nucleated samples belongs to 3rd stage nucleation samples, that have undergone oxygen plasma treatment, reaching $3.20\text{E}+11$ or $3.20*10^{11}[\text{cm}^{-2}]$

Primary sources of Si-V color centers in diamonds are the sp₂ hybridized carbon atoms, that demolish the sp₃ diamond crystal lattice and connect the nearby crystallites together.. These defects are primarily found in the interfacial regions or in other words in grain boundaries, between the diamond crystallites and they greatly affect properties and characteristics of NCD films. Raman spectroscopy is optimal for observing and characterizing them, since sp₂ hybridized carbon atoms possess a high Raman scattering cross-section.^[5] And this observation is important, as it determines that further practical applications of NCD films. Its characteristic on the Raman spectrum is a slight peak at $\sim 1339[\text{cm}^{-1}]$ with x-value representing the wavelength and y-axis representing the intensity in auxiliary units (a.u.) or unitless in some cases. There is also G and D band gaps of sp₂ orbitals that we can observe at $1330\text{-}1380[\text{cm}^{-1}]$ and $1550\text{-}1600[\text{cm}^{-1}]$, although position of such peak varies depending on the excitation energy of the material.^[6]

Photoluminescence spectroscopy will help in characterizing the Si-V properties in the form of a peak on the spectra (intensity[a.u.]/wavelength[nm]). In order to seek application of NCD in biosensing we have to observe and make sense of the changes in photoluminescence properties of this peak and how the chemicals affect it. Thickness of the NCD deposited and nucleated films as well as relative thickness of the chemicals is measured using state of the art optical Raman microscope with the configuration of AFM (Atomic force microscopy). Materials that are used for drop-casting are chemical solutions of BSA and FBS in the 30mg/ml

ratio. The chemicals are frozen, they reside in the freezer under 0-3°C as unfrozen they won't influence the PL characteristics. Under impact of oxygen, solution goes into reaction involving it and loses some of its important properties. So, after we unfreeze and drop-cast the chemicals on top of the NCD layer, we immediately put them back in the freezer.

1.1 – “Standard” vs “Fine” nucleation method and first steps

Before we start with the experimental description, it is first important to outline the difference between the “standard” and the “fine” nucleation methods. During the nucleation process, the samples undergo a process of rinsing in DnD (Detonation nano-diamond) solution. The solution is created from mix of the water and the DnD powder in 2mg / 1ml ratio. After its creation, due to the powder being impure to some extent, the liquid DnD will be muddy. The unfortunate result of such solution is that in theory, during the process of deposition, known as the growth off the NCD (nano-crystalline diamond) layer, the layer will be thicker (>50nm) as the grains during nucleation become more agglomerated. Such is the “standard” procedure of nucleation of samples.

“Fine” method of seeding follows approximately the same procedure, the only difference from the “standard” is the purifying of the DnD solution. To remove the mud from this liquid, we first decluster it. Then, we put it through the centrifugation process, 3 times in a row, to purify the DnD solution and remove the unwanted residue. 6 probes with DnD solution were spun in the centrifugal machine (Benchmark MC-12) with a room temperature (22-23°C) and 5,000 – 15,500[rpm] at a time. And only after this can we rinse the samples in this purified solution and the results are the “fine” method nucleated silicon samples. On the surface of the nucleation the grains will be denser and the layer after growth in the deposition chamber will be thinner (<50nm). “Fine” method is ideal for us, because we want to observe the Si-V peak on the NCD surface, which is significantly harder to do on the thicker layer.

We start by preparing the pure silicon samples. This substrate is very common in the field of nanodiamond layer growth, as it is easily accessible, has low stress induced after the growth and good adhesion. The samples are divided into two sections: the ones that would be used for “standard” nucleation method and the ones that would be used for the “fine”. The “standard” method samples were cut by the special laser and delivered to FZU, so the samples are precisely 10x10[mm] squares. Silicon samples for the “fine” method were cut by me as accurately as possible with a special diamond tip pencil (5x10mm). All the silicon samples have a crystallographic dimensions of <1,0,0>.

There would be 12 samples for the “standard” with the length and width of 10[mm] and 36 samples for the “fine” nucleation method with the 5x10[mm] properties. This is for a reason that it would be beneficial to show differences in the NCD layer of both after deposition process.

Next step is cleaning of the silicon samples from dirt and smaller unwanted particles. The process is very thorough and utilizes an ultrasonic bath (Elmasonic S30, Power source: f = 50-60Hz; power = 220-240V; working f = 37kHz). Such baths are often used in sonochemistry. It is filled with the DI-water and the walls are covered with stainless steel. It is used for cleaning hard materials by removing the cavities from its molecules.^[7] The samples of course will not be a rinsed without a sample holder, positioned in the cup. This is a many steps

procedure: we first fill the cup with Acetone and put it into the ultrasonic bath for 10 minutes. It is important to note, that the liquid inside the cup should be the same level as water in the US-bath, otherwise the cleaning would be inefficient. Then we clean the samples inside the cup with deionized water and repeat the process of US-bathing for 10 minutes, but with isopropanol this time. Due to safety reasons, we pour used acetone and isopropanol back to their respective containers. The samples are rinsed with DI (deionized) water one more time and blow by Ni (nitrogen) pistol for drying.

1.2 – Oxygen plasma

Oxygen plasma treatment is any plasma treatment with addition of oxygen, it is essentially used for cleaning the surfaces prior to bonding. Oxygen is known for cleaning organics and non-metals (e.g., plastics) and has the capability to modify the surface of material.^[8] It can also clean metals if mixed with Argon (Ag). Prior to nucleation, half of the samples undergo an oxygen plasma treatment or oxygenation. In all cases the parameters are: oxygen plasma for 4[minutes] under 100[W], frequency tuning is off, and the frequency is 8000[kHz]. Only oxygen is introduced to the system, as Silicon (Si) is a non-metal. The process starts with the chamber pumping down, and after this O₂ flows inside the chamber. During the process of oxygen plasma treatment, the plasma must not be pink-coloured, as it would mean that leftover gasses or air are still inside, and the process would be stopped immediately. The oxygen plasma has a grey, almost blueish colour, which could be noticed through the glass of oxygen plasma device. The device used is from FZU (University of Physics in Prague), with a software of the “SVCS process innovation” company.



[Figure 4.1: Oxygen Plasma inside the chamber, ran under 100W for 4 minutes]

Prior to loading the chamber with the samples, if the system hasn't been used for a long time, we first run the same process of oxygen plasma treatment (4minutes, 100W) for the empty chamber, for cleaning purposes. Overall, we treated 18 silicon samples of the "fine" method nucleation and 6 for the "standard" with oxygen plasma. For simplicity reasons, the samples called Si will be the non-oxygenated silicon samples, while the O-Si are the ones that have undergone oxygen plasma treatment.

1.3 – Preparation of the DnD solution

The DnD is the detonation nanodiamond, that is produced from the carbon contained in high energy explosives. The usual size of its primary particles is about 4[nm]. "DND had also been employed for seeding substrates used in the CVD growth of diamond films.". [9] This is the reason why we will rely on it, or rather on the solution made from its powder, where we will rinse the samples in order to nucleate them. DnD solution prepared for the "standard" method was made without purification meaning the layer after the deposition will be thicker. But in order to observe the Si-V peak we need a thinner layer, so for the "fine" nucleation method we will perform steps necessary to remove mud from the solution. First, we take the DnD powder in the quantity of 961.5[mg] and we need to oxidize and hydrogenate it before making a solution. The process took 30 minutes for the DND to oxidize and about 3 hours for the chamber and the powder itself to cool off. The initial 30 minutes were running under the extreme temperature of 520°C. The reason this step is important is due to diamond particles having the outer layer of sp₃ orbitals, or in simple terms - graphite. Oxidization removes the layer of sp₂ and even some of sp₃, which is part of the diamond particle.

After oxidization we end up with 530mg of DND powder, compared to initial 960mg, meaning that we lost approximately 430mg in the process and now it must undergo the process of hydrogenation in quartz oven. This is important, because the process pushes the pure diamond grains(sp₃) closer to each other by hydrogenating them. When grains are near one another, there will be less empty space left during the creation of the nanodiamond layer and the layer will be more homogenous. Hydrogenation can also be done in the deposition chamber, which is how we create the nanodiamond layer later, but not under the temperature as high and not with special containers with rods for the powdered substance. We start the hydrogenation for O-DND 520/30. The process of hydrogenation takes 3 steps. Pumping of the chamber, so that the vacuum is created and preserved inside, and the leftover gasses and air are absolved of. The heating, up to 700°C in our case, which is the longest step, taking approximately 6 hours. And finally, the cooldown, about 5 hours. So, in total the process takes at least 13 hours. We get the hydrogenated DND out of the oven and find that its weight decreased from 530mg by ~104mg, leaving us with approximately 426mg of the DnD 520/30-H powder. During these processes, DnD powder loses its mass, so we had to use a large amount. We have 36 samples for "fine" nucleation, if we put 2 samples in one probe with 2ml of solution with the centrifugation process running 3 times and the required 2mg/ml ratio and 48ml of water, we need 96[mg] of the powder. We take 96.1[mg] of DnD 520/30-H and mix it with 48[ml] of DI-water.



[Figure 1.3: Microcentrifuge "Benchmark MC-12"]



[Figure 1.2: Ultrasonic probe "Dr. Hielscher UP300S"]

The following step is to decluster the DnD solution, by the ultrasonic probe (Dr. Hielscher UP200S Ultrasonic Homogenizer Disperser Sonotrode S14 Homogenisator, Power source: $f = 50\text{-}60\text{Hz}$; $V = 230\text{V}$; max working $f = 24\text{kHz}$), also present on the Figure 1.2, under the power of $200[\text{W}]$, which is also a limit of the device. Procedure took 1 hour. Such probe has an ultrasound tip/horn that resides in the solution during the whole process. Due to the volume limitations, we can only decluster $24[\text{ml}]$ of the solution at a time. Device works by generating and transmitting the US-waves to the solution by the ultrasound tip.

Next, we must centrifugate the solution in the special microcentrifuge, present on the Figure 1.3 (Benchmark MC-12, Max speed = $15,500\text{rpm}$; Max capacity (2ml probes) = 12), that will rotate the solution inside probes (2ml each) at high speed of $14,500[\text{rpm}]$ and average room temperature($22\text{-}23^\circ\text{C}$) and after 1 hour and 30 minutes, the process ends and for some time the unwanted mud or dirt will settle on the bottom of the probe. Then we carefully suck the $1[\text{ml}]$ of the solution on top with a micropipette (CAPP Bravo) and fill new probes with $2[\text{ml}]$ of it for each. This process must be repeated 3 times, with the same parameters, leaving us with 6 probes of pure DnD 520/30-H declustered DnD solution, $2[\text{ml}]$ each. Even though we separated the residue from the "fine" DnD solution, it has to be used for nucleation in the nearest time, otherwise the nucleation will result in a thicker layer and the whole purpose is ruined.

1.4 – Nucleation

Only the top side of the silicon samples will be exposed to seeding, so we will put 2 samples of Silicon in each probe back-to-back. Nucleation for the "standard" method is different than that of the "fine" one.

For the “standard” method nucleation, we take the pre-prepared solution of 520/35-H that was not purified and flow it in a cup with the 10x10[mm] samples inside. Then we put it into the US-bath for 10 minutes. Then thorough cleaning of the samples with water is necessary, after which we dry them with Ni (Nitrogen) pistol for approximately 1 minute.

For the “fine” nucleation method we have 3 different stages of nucleation. We put 2 silicon samples in each probe, filled with 2[ml] solution of pure 520/30-H DnD and expose them to the US-bath for 10 minutes. Every time we do this process, we get a respective stage of nucleation (1st time – 1st stage, 2nd time – 2nd stage, etc.). It is expected that stages 2 and 3 will be the most reliable with the highest density, since the solution in the first stage is very concentrated and the nucleated layer, although might be relatively dense, will have many agglomerated grains of NCD. Same is true for the 4th seeding stage, which we will not perform for this reason. Such grains, though, can also appear at the 2nd and 3rd stages, but to a much lesser extent. Between the 2nd and 3rd stages it is unclear which one is the best in terms of density, so we will perform SEM (Scanning Electron Microscopy) analysis on all three and compare the nucleation density (in chapter 2). We prepare 6 samples of Si and O-Si for every nucleation step up to the 3rd (included).

Although the grains on the nucleated surface are those of the nanodiamond, the nucleation is not as strong before deposition. Hence, the samples must be handled carefully, as upon contact with any surface, there is a high chance that the nucleation layer could be destroyed. Our result is 12 “standardly” nucleated samples (6 O-Si and 6 Si) and 36 “finely” nucleated samples: 6 for Si and 6 for O-Si of the 1st, 2nd, and 3rd stages of seeding.

The very last step of nucleation is making a cross sectional scratch in the shape of a plus on the nucleated surface. This scratch will be useful at different stages of the work, for example focusing on the sample surface during PL and Raman stages, which can be hard due to its monochromatic characteristics. But the most important is the AFM topography scanning, as it reveals to us the difference between the layer of deposited NCD and the silicon. During the process of CVD, the nucleated surface will grow, but the grains that can appear on the scratched surface are very minimal. So, the scratched surface will most reliably show the pure silicon layer. We must not make this scratch after the deposition. Not only is the NCD layer very rigid and some of it can stay, but the scratched surface will also move to the sides and the height will turn out to be incorrect.

Chapter 2

SEM

20

2.1 – What is SEM

SEM is a short term for Scanning Electron Microscopy and compared to the conventional optical microscope with the resolution of 1000x, in other words one that can measure only down to the area of $200[\text{nm}^2]$, can measure the area much lower, down to approximately $2[\text{nm}^2]$ and has a magnification of 1,000,000x. The resolution of SEM microscope goes up to 1[nm].^[10] A focused stream of electron of large energy levels are projected on the sample with a solid structure. The technique has many uses, namely it can reveal the topography and morphology of the said sample, chemical composition, and crystalline structure along with crystalline orientation. SEM is also capable of measuring specific points and parts of the sample.^[11]

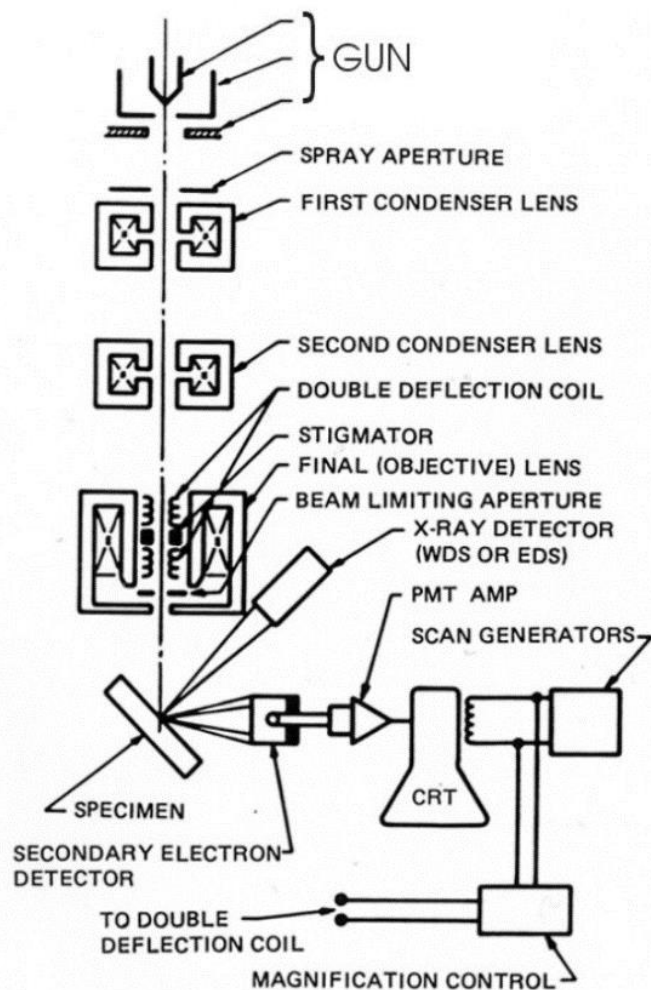


[Figure 2.1: Schematic drawing of the electron and x-ray optics of a combined SEM-EPMA]^[11]

2.2 – How SEM works

In SEM the source of electrons also called the “gun” emits electrons that can reach very high energies of up to 1000[kEv] (kilo ElectronVolts), alternatively the wavelengths between 0.027[nm] and 0.0009[nm]. [10]

The electron-sample interaction is a process when accelerated electrons make contact and start a reaction in the atoms of the target sample they are directed to. Such electrons carry kinetic energy and when this interaction occurs, with the loss of initial acceleration of the first, the energy transforms into different signals. [10]

There are two types of electrons that are common in scanning electron microscopy: the secondary electrons and the backscattered electrons (BSE in short), both of which appear as a form of mentioned signal. Secondary electrons are electrons that escape from the sample, carrying energy below 50[eV], mainly knocked out of their atom orbit by other electrons. They are useful from scan of the morphology and topography and the BSE show differences between compound of the multiphase samples. The BSE (backscattered electrons) are electrons that create secondary electrons. They get close enough to the core of the atom to knock them out of the atom’s orbit. By the impact they scatter through a large angle and emerge from the surface again. They aren’t as numerous as the secondary electrons, but they do have higher energy. [10][11]

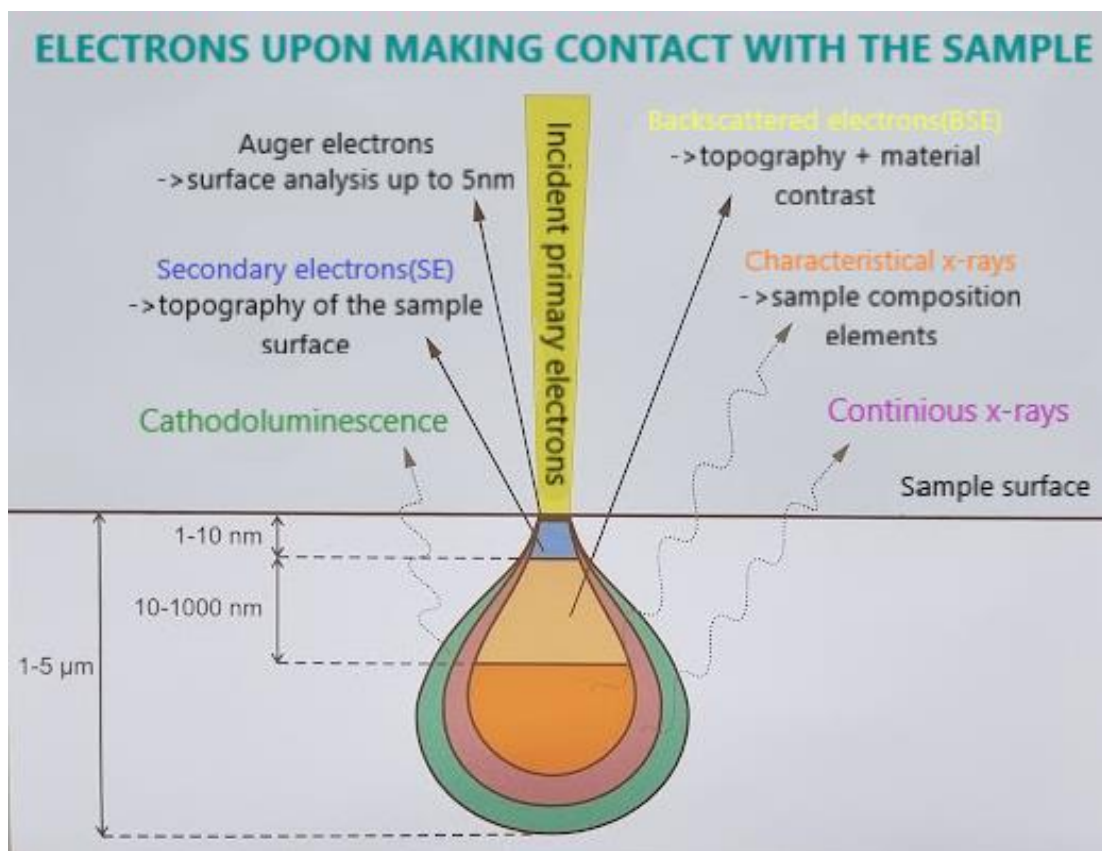


[Figure 2.2: Process of incident electrons contacting the sample's surface]

The image in SEM is created when the accelerated focused beam of electrons contacts the sample surface. As presented on the Figure 2.2, schematic taken from the FZU university, the beam of incident electrons is directed onto the specimen's surface, which result in the scattering of different types of electrons, which are detected as the signal. These signals give insight of different material properties. The already discussed secondary electrons are great for measuring topography of the sample, they are very important for us as we will be taking scans of the nucleated samples, where topography is essential. Although, few backscattered electrons are caught by the detector that observes secondary electrons, some compositional contrast is also present.^[10] Secondary electrons scatter from places close to the surface of the material(1-10[nm] in depth as presented in Figure 2.2) and as such they have higher resolution than those that scatter from deeper levels (e.g., BSE).

There are much less BSE than secondary electrons, but they have energy much higher. Images have less resolution as they scatter from deeper levels of the specimen, from the depth of 10-1000[nm] (Figure 2.2). They provide crystallographic data and some material properties as well as topography.^[10] From the same depth the x-rays scattering occurs. When the incident electrons knock out an inner shell electron and an outer-shell electron takes its place, electrons' traversal from higher to lower energy levels takes place. The process is constant until all the energy states are refilled and every step the x-rays scatter in order to conserve energy. When a wavelength-dispersive or an energy dispersive spectrometer, which is more common in SEM, observe the x-rays we get information about the chemical composition of the sample.^[10] There are also x-rays coming from very large depths (1-5um) as demonstrated in the Figure 2.2.

Auger electrons are emitted from the same depth as the secondary ones and give valuable information about the surface chemistry of the sample. In order to achieve a signal of such electrons, high quality detectors are required, and they aren't commonly used. Once the conditions are met, we can get detailed analysis of the sample's surface up to 5[nm].

2.3 – SEM microscope structure

One of the main components of SEM is an electron gun. It has 3 types:

- 1) The tungsten hairpin filament. Current passes through it and produced temperature of over 2500 degrees Celsius results in the emission of electrons from its tip. [10]
- 2) The Lanthanum Hexaboride (LaB_6) filament. With the expense of a “brighter” beam, due to the larger beam current, the lifetime of such filament is much shorter than that of the tungsten hairpin one. They are also more expensive. [10]
- 3) Field emission guns or in other words “cold cathode” emitters. Very high electric field is applied to the tip, directed precisely to the sample, until quantum mechanical tunneling occurs. “Quantum mechanical tunneling is a consequence of the wave nature of particles that implies that a particle can penetrate a potential energy barrier even though there is insufficient energy to overcome it”. [12] More expensive, because unlike the predecessors that require a pressure of 10^{-6} [Torr] or approximately $13\text{E-}4$ [Pa] to create a vacuum near the gun, it requires 10^{-10} [Torr]/ $1.33\text{E-}7$ [Pa]. They also don’t use heat, which is how they got their second name. [10]

Table 1 illustrates the differences between them in more details.

[Table 1: Features of three electron guns]^[11]

	TE gun		FE gun	SE gun
	Tungsten	LaB_6		
Electron-source size	$15 \sim 20 \mu\text{m}$	$10 \mu\text{m}$	$5 \sim 10\text{nm}$	$15 \sim 20\text{nm}$
Brightness ($\text{Acm}^{-2} \text{rad}^{-2}$)	10^5	10^6	10^8	10^8
Energy spread (eV)	$3 \sim 4$	$2 \sim 3$	0.3	$0.7 \sim 1$
Lifetime	50 h	500 h	Several years	1 to 2 years
Cathode temperature (K)	2800	1900	300	1800
Current fluctuation (per hour)	<1%	<2%	>10%	<1%

The upper part of the microscope is called “cathode” and it is essentially a sharp wolfram tip. Electrons get sucked from it and move through two more parts of the microscope column: “condensers” and the “objective”. As demonstrated on the Figure 2.1, the first part of the “condensers”, below the electron source gun is the first and second condenser lens. There are 2 lenses in the microscope, the mentioned and the objective lens located in the “objective” column. These lenses allow us to control the diameter of the electron beam. When the electron beam from the electron gun is focused by the two-stage lenses, a small electron probe is created. When the condenser lens fortifies its action of the lens, the electron probe widens.

Close to the end of the microscope column there are stigmators. There is a process called astigmatism, it is when the lens has varying strengths as a function of the rotation around the lens axis, so instead of a single point focus we get a two-line focus, which makes the stream of electrons the shape of an ellipse. Stigmators are present to fix astigmatism of the electro lens and shape the electron beam back to circular form. [14]

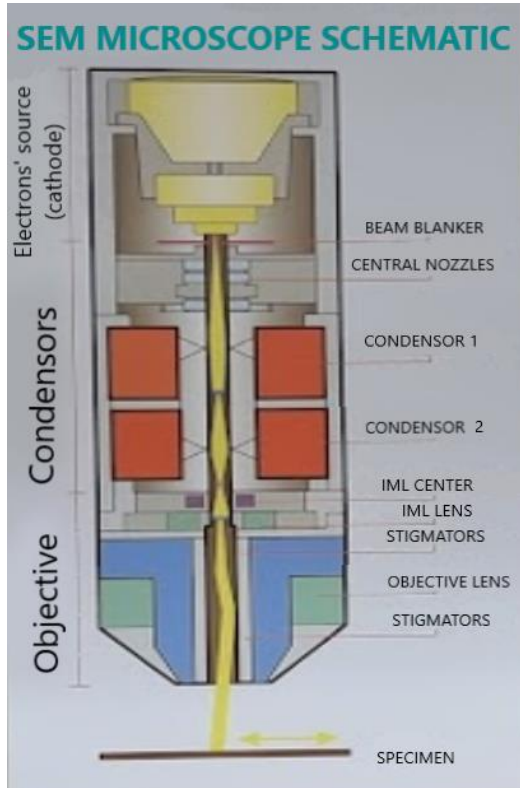


[Figure 2.3: SEM microscope schematic]



[Figure 2.4: Scanning Electron Microscope MAIA(Tescan)]

The SEM we will be utilizing in FZU is of the model Scanning Electron Microscope MAIA3(Tescan) presented on Figure 2.4. It has detectors to control the direction of the secondary electrons and BSE. Its resolution reaches 1nm at 15kV. It could also be utilized for analysis of elemental properties of the specimen using EDS (Energy-dispersive X-ray spectroscopy).^[15] Its column schematic was taken from FZU (Institute of Physics) located in Prague 16200, Cukrovarnicka 10 (Figure 2.3).

Before measuring the samples, we have to create vacuum inside the chamber. Because the beam of electrons has to be precise, nothing should obstruct and disturb it, so it must be created and preserved there. The constant stream of electrons will cover the whole observable area of the specimen, moving from one point to another, creating the SEM scan or the SEM image of it. We are interested in topography, so we will rely on the secondary electrons only. We can't use optical microscope because its resolution is enough to measure an area of 200[nm^2] max, whilst the SEM microscope measures an area as small as 2[nm^2] approximately. This is ideal for us because the average diameter of the nucleated grain is 5-10[nm].^[2]

2.4 – Measurement steps

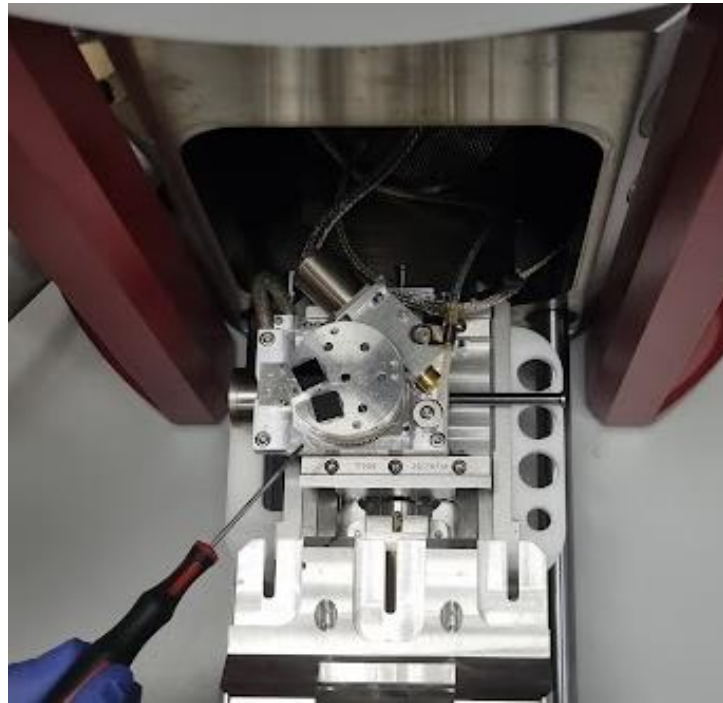


[Figure 2.5: Seeded Si samples placed on the SEM wafer]

After we unscrew and open the chamber of the SEM microscope, we see a drawer with a special wafer inside for the specimen. On the Figure 1.5 we can see the 2 already set nucleated/deposited 10x10[mm] samples of the “standard” method nucleation. After we open up the software there are 4 steps we have to do in this order:

1) Auto gun centering:

Gun centering centers a stream of electrons to be positioned in the middle of the microscope column. It is formed by a system of electromagnetic deflection coils under the gun. Its intention is tilting the electron beam that the gun emits, so that it is aligned with the optical system of the column.^[16] The function of auto gun centering that can be accessed by “*adjustments -> auto-gun centering*” and it helps with centering the gun optimally by an automatic function.

2) Beam intensity and acceleration Voltage setting.

During the auto-gun centering the beam intensity and the absorbed current change haphazardly. As instructed, the acceleration Voltage is set to 15[kV]. The value we used from beam intensity on the other hand is dependent on the absorbed current and the absorbed current does not have a constant value in our case, as it changes during the observation. We set this beam intensity high only if the samples aren’t very sensitive, so they don’t get destroyed. Then we try to focus on the sample with a special spherical joystick, changing the working distance (the distance from the very end of the microscope to the sample surface) in the process.

3) Manual column centering.

The third step is the manual column centering. It is for the stream of electrons to be exactly in the center, otherwise the image would wobble strongly, and no scan can be taken reliably. This happens due to defects of the electromagnetic lenses. The uncertainty of the image can be fixed during this stage, but it is unavoidable for higher magnifications (e.g., 300kx). For an instance: absorption current is 102[uA] during this step and the working distance is 9.448[mm].

4) Focus.

The final, fourth step, is to focus on the scratch we made after nucleation. We do it for convenience. As the scratch and the nucleation layer have different contrasts, the focusing is easier. We must fixate the scan of the surface in both axes individually. First, we start with the y-axis. With the help of the spherical joystick, the image becomes sharper and clearer, but the joystick is very sensitive, which required us to change between aligning the x and y axis. If the image moves from left to right and vice versa during the process, then we change the x-axis. If it moves from top to bottom, and the other way around, then the y-axis. Moreover, staying on one spot for a long time burns it which results in its darkening. This makes aligning hard, so we have to be quick or change the spot in the process. It is also possible to choose a smaller area of the scan and try to focus using only that piece.

After all the steps are done and the signal image of the sample is sharp enough (it is never too sharp for higher magnifications, so no need to be extremely precise), the microscope can move around the chamber by the spherical joystick to observe different samples without pumping down and opening the chamber to change them.

2.5 – Experimental section

On the 8th of May 2022, we do SEM observation for the earlier prepared 1st, 2nd, and 3rd stages of “fine” method nucleation on top of the pure Si samples. This measurement will be done for both Si and O-Si (those that have undergone oxygen plasma prior to nucleation) samples. We want to see the difference between the density of nucleated Si and nucleated O-Si samples and determine which are better, as the denser the surface, the more complete and thinner the NCD layer will be after the deposition.

The SEM scan of 200kx magnification of the Si group of 1st, 2nd, and 3rd stages of “fine” seeding method can be seen on the Figure 1.6 and the one for O-Si group is on the Figure 1.7. The samples were measured under the parameters: $V_{\text{acceleration}} = 15[\text{kV}]$; $I_{\text{absorption}} = 107[\text{pA}]$ for the 3rd stage, 90[pA] for the 2nd stage and 102[pA] for the 1st stage. The WD (working distance) is 4.51[mm] in the first, 4.35[mm] in the second and 4.54[mm] in the third stage of nucleation of Si group and WD is 5.43[mm] in the first, 4.43[mm] in the second and 4.31[mm] in the third stage of nucleation of O-Si group. The working distance has minimal effects on the difference between scans when the difference is below or approximately 1[mm], as it is in our case.

The view field of the SEM scan is always 0.948[um] for all the images of the samples in the 200kx magnification, which I decided to use for the silver lining between quality of the image and the smallest area with sufficient quality, as it is easier to count the number of grains there. The contrast in Figure 1.7 between stage one seeding(left-most) and the other two differs slightly as the first one is brighter. This does not have any influence on the difference between scans and the number of grains and is just a visual issue.

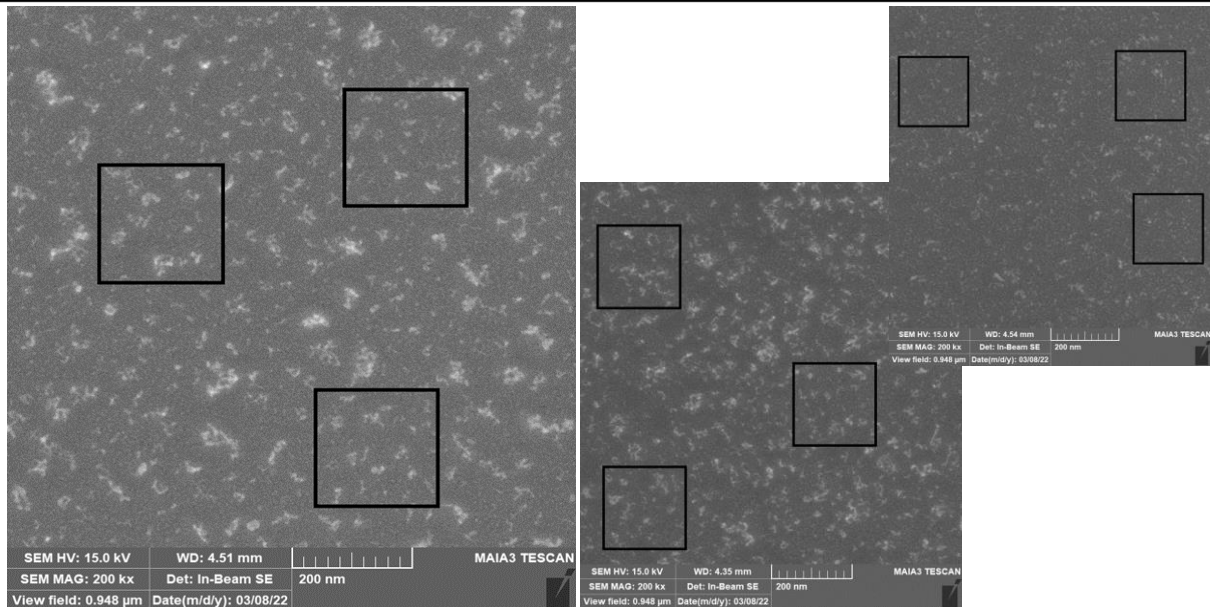


[Figure 2.6: SEM scan of O-Si nucleated samples of 1st, 2nd and 3rd stages (left to right respectively)]

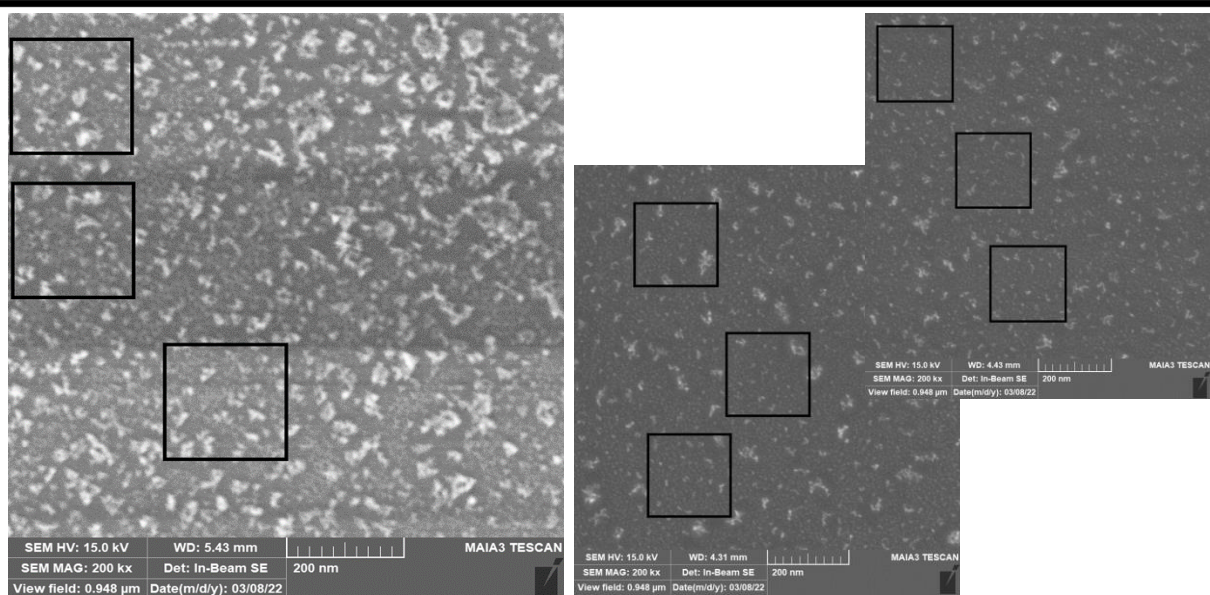


[Figure 2.7: SEM scan of Si nucleated samples of 1st, 2nd and 3rd stages (left to right respectively)]

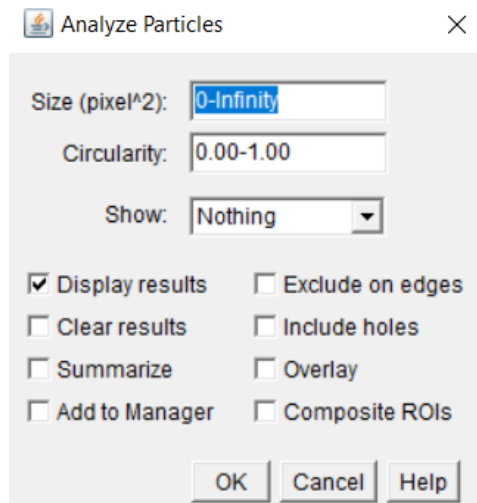
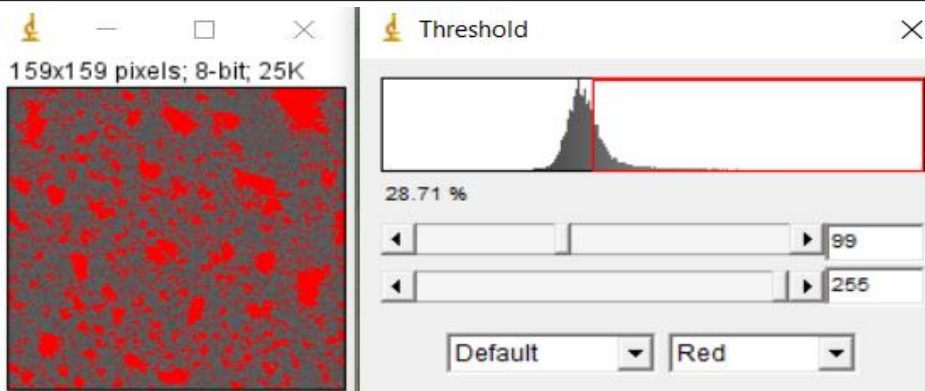


[Figure 2.8: Analyze particles option]

The squares I highlighted on the Figure 1.6 and Figure 1.7 are sections that I took for measuring the amount of nucleated NCD grains and ultimately calculating the density of the seeding on the samples with them. The areas are 200x200[nm] and the scale of 200[nm] from the SEM scans was used as a reference for their evaluation (Figure 1.6 and 1.7 in the bottom).

As counting the number of grains on each of the scans manually is time consuming, instead I decided to use ImageJ (The version of the software that was used is 1.8.0_172.). ImageJ software is mainly used by people working in the chemistry-related activities. Its main feature that we will utilize is counting the number of particles of a certain area/diameter from the image. Size of the area can be set in the software itself following the path “*Analyze -> Analyze particles*”. It is important that we convert the image to the 8-bit scale, or in other words, to the black and white. The shortcut to that command is “*Image -> type -> 8-bit*”. The scans only have 2 colors so it will not have a huge impact, however some smaller particles could still be lost due to the quality of the 200x200[nm] areas taken separately, but there is no other method that could resolve this issue. However, ImageJ only has [pixels²] as the available unit for the input (Figure 1.8), so in order to utilize this feature I converted the size of some grain from [nm] to [pixels] (Pxls). To measure its diameter, I took the scale in the bottom of SEM scan (200[nm]) and measured the grain that was exactly the size of one of its line segments for simplicity. Its diameter is exactly 20[nm]. From that information I counted diameter as the number of pixels in the simple graphic art program. So now we know that its diameter is exactly 17[pixels]. So, 20[nm] = 17[pixels]. The average smallest grain found on the scan is approximately 5.88[nm] in diameter, which is also 5[pixels]. But this is not enough, since ImageJ requires the [pixels²] unit, so we use the circle area formula 1 after converting to pixels from nm:

$$S = \pi * \frac{d^2}{4} [\text{pxls}^2] \quad (1)$$



For example, for approximately 5.88[nm], the pixel size is determined to be 5[pxls] and so the area of the grain would be close to 19.6[pxls²]. I round it up to 20[pxls²], and input as the minimal pixel size, while the maximum is infinity. After this we must adjust the threshold for proper NCD grain distinction from the Si surface and the contrast I chose had to be picked by personal bare-eyed observation, so I chose as reliably as I could. The option is present on the Figure 1.9 along with the contrast I chose for all the sectional areas.

The final step is to set the minimal pixel² number for the particles analysis and run the program. And the program highlights all the particles that fall in this category. In the figure 1.10 is 3 images from different stages of the work in imageJ and the last one (c) is the one with highlighted and numerated grains. More importantly, however, the software counts all of the particles and gives the total number of them. From this, we can get the density of the nucleation/grains, using Formula 2.

The area is always 200x200[nm], which is 40,000[nm²] of these sections and 3 sections were taken from each sample. For example, the Si sample of the first stage nucleation has 51, 45 and 50 grains in three 200x200[nm] sections of its scan, so we take the average, which will be approximately 48.7[-] grains. Using the Formula 2 we get exactly 0.0012175[1/nm²]. This number correlates to the density of nucleation of said sample. Then we convert it to [1/cm²], because this is the units mostly everyone uses and would understand much better for the density case. The final value is 1.22 * 10¹¹[1/cm²].

$$\rho = \frac{\text{quantity of grains on the area}}{\text{area of the scan}} \left[\frac{1}{\text{nm}^2} \right] \quad (2)$$

Measuring density of 1 sample is not enough as we need to compare the densities of 3 different nucleation stages as well as observe if oxygen plasma prior to seeding influences this as well. The Table 2 illustrates different densities for various nucleation stages and samples. The reason for additionally measuring it for more than one minimal grain size in diameter is to establish if there is a significant difference between them in that regard. A table of [nm] to [pxls] conversion, manually created, is present on the Figure 1.11.

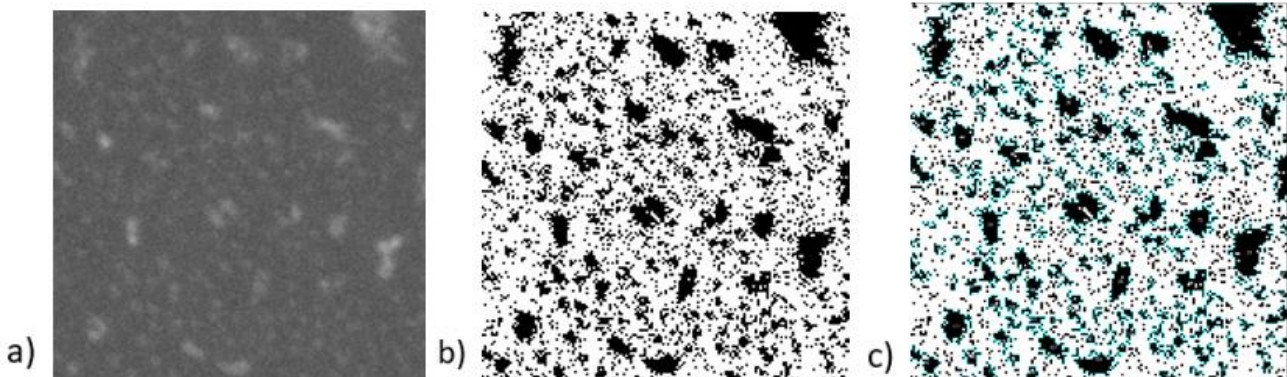


[Figure 2.10: a - SEM image of 3rd stage Si “fine” nucleation; b - 8-bit scale of the said image after changing the contrast by threshold command; c - the highlighted grains on the scan after setting the maximal pixel size; all the images are in a 200x200[nm] area]

[Table 2: Density of the grains in O-Si (oxygenated prior to seeding) and Si samples in 3 nucleation stages from the minimal grain size of 2[nm] to 7[nm] in diameter with 1[nm] step and also 10[nm] in diameter (pxls² is pixels)]

Density [1/cm ²]	2[nm] diameter or 2.27[pxls ²]	3[nm] diameter or 5.11[pxls ²]	4[nm] diameter or 9.08[pxls ²]	5[nm] diameter or 14.19[pxls ²]	6[nm] diameter or 20.43[pxls ²]	7[nm] diameter or 27.81[pxls ²]	10[nm] diameter or 108.71[pxls ²]
1st stage Si	2,4083E+11	1,3917E+11	1,1750E+11	1,0333E+11	9,4167E+10	8,5000E+10	5,0833E+10
1st stage O-Si	2,5667E+11	1,1000E+11	7,9167E+10	5,9167E+10	5,0000E+10	4,3333E+10	1,9167E+10
2nd stage Si	6,2750E+11	4,3417E+11	3,1083E+11	2,1667E+11	1,5500E+11	1,1417E+11	2,5000E+10
2nd stage O-Si	6,7167E+11	2,5500E+11	1,3500E+11	9,8333E+10	7,5000E+10	6,5833E+10	2,7500E+10
3rd stage Si	7,2417E+11	4,0250E+11	2,7917E+11	2,0083E+11	1,4333E+11	1,0333E+11	2,4167E+10
3rd stage O-Si	1,1200E+12	5,2833E+11	3,2000E+11	2,1167E+11	1,4750E+11	1,0667E+11	2,1667E+10

From table 2 we can see that the density of the nucleation is generally smaller for the first stage, than for the second and third, only slightly overtaking when the smallest diameter is set to 10[nm] and higher. The problem with it is that it also has the highest amount of very large grains, that would interfere with the creation of the thin layer as they would grow to be much thicker during deposition, so we will not expect a thin layer from it. Although there are not many differences between Si and O-Si in the 1st stage for the lowest minimal diameter of 2[nm] and 3[nm], the density of O-Si tends to be much lower than the one of Si, as the minimal diameter increases.

Regarding stages 2 and 3, the density seems to be higher for smaller minimal diameter for both Si and O-Si, with 3rd stage nucleation O-Si density reaching power of 10¹². It diminishes as the smallest diameter is increased. This means that there are more grains per area, and lesser large grains, which is supported by manual observation. Between Si and O-Si, for stage three the Silicon oxygenated prior to nucleation has a higher density, than the one that wasn't. But for the second stage it is the other way around. The lowest difference there is in the minimal diameter of grains as 2[nm] and 10[nm], otherwise, it is significant.

$$2\text{nm} - 1.7\text{pxls} \rightarrow 3.14\text{nm}^2 - 2.27\text{pxls}^2 \sim = 2\text{pxls}^2$$

$$3\text{nm} - 2.55\text{pxls} \rightarrow 7.07\text{nm}^2 - 5.11\text{pxls}^2 \sim = 5\text{pxls}^2$$

$$4\text{nm} - 3.4\text{pxls} \rightarrow 15.57\text{nm}^2 - 9.08\text{pxls}^2 \sim = 9\text{pxls}^2$$

$$5\text{nm} - 4.25\text{pxls} \rightarrow 19.63\text{nm}^2 - 14.19\text{pxls}^2 \sim = 14\text{pxls}^2$$

$$6\text{nm} - 5.1\text{pxls} \rightarrow 28.27\text{nm}^2 - 20.43\text{pxls}^2 \sim = 20\text{pxls}^2$$

$$7\text{nm} - 5.95\text{pxls} \rightarrow 38.48\text{nm}^2 - 27.81\text{pxls}^2 \sim = 28\text{pxls}^2$$

[Figure 2.11: Minimal grain size conversion from the data in table 2, from nm to nm² and pxls and from newfound pxls to pxls² with approximation to integer (pxls = pixels)]

From the **AFM scan Figure 4.13** which will be also later explained in the AFM section, we take the average of all the grain sizes. The average size of the grains there is 4[nm], which is also in Table 2. From the table values we make a graph for density comparison with 6 points for 3 stages of Si and O-Si (Figure 1.12). Density of the 3rd stage of Si and O-Si is the highest, reaching approximately 3.00E+11 [1/cm²], with O-Si being denser. 2nd stage's density is also approximately the same value for Si, but the O-Si is enormously lower, close to 1.50E+11 [1/cm²]. And finally, 1st stage has the lowest density, with O-Si lower than Si.

SEM measurements of “standardly” nucleated samples was performed as well and will be expanded upon in the conclusion(Chapter 5).

2.6 – Results

In conclusion, oxygen plasma was successful and resulted in a dense layer for the silicon samples, that were nucleated by the 3rd stage pure DnD solution and for the other stages (2nd and 3rd) it took the worse effect., so suggestion would be to use oxygenation on the silicon samples that would only be used for the 3rd stage nucleation. Aside from that, the density of the nucleated samples with the smallest grains of 4[nm] (also present on the Figure 1.12) for 3rd stage is the highest for both Si and O-Si. This represents a large number of particles on the 200x200[nm²] area of the sample. In other words, higher density means more composition, unless the larger grains are present and are very dominant. In the case of 2nd and 3rd stages of seeding, fortunately had only a few, unlike the 1st stage. Figure 1.13 shows this comparison, the density of the 1st stage is lowest for both Si and O-Si at 2[nm] lowest particle diameter, but at 10[nm] it has the largest, meaning larger grains are dominant on the scans. For the 2nd stage there is a strange instance of O-Si density value being more than 50% lower than the value of Si sample, which is almost the same as the 3rd stage density value. This means that

both 2nd and 3rd stages of nucleation are useful for creating thin NCD layer during deposition, while on the 1st stage of nucleation we expect a NCD layer of more than 50[nm].

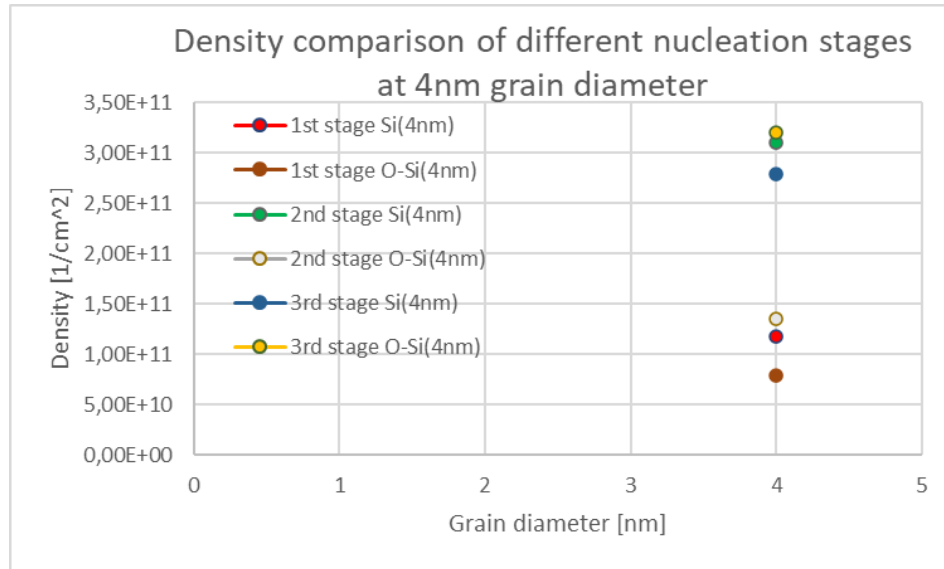


[Figure 2.12: Density comparison for minimal grain diameter of 4[nm] at different nucleation stages for Si and O-Si]

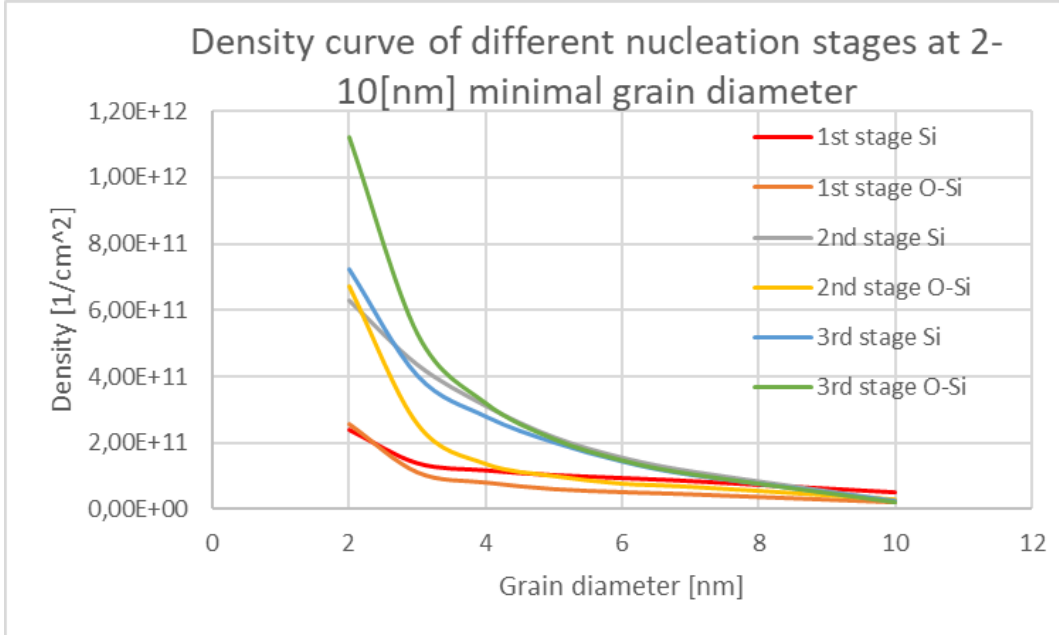


[Figure 2.13: Density curves of 3 nucleation stages for Si and O-Si samples, that show changes in density in regard to the minimal grain diameter]

Chapter 3

CVD

33

3.1 – What is CVD and how does it work

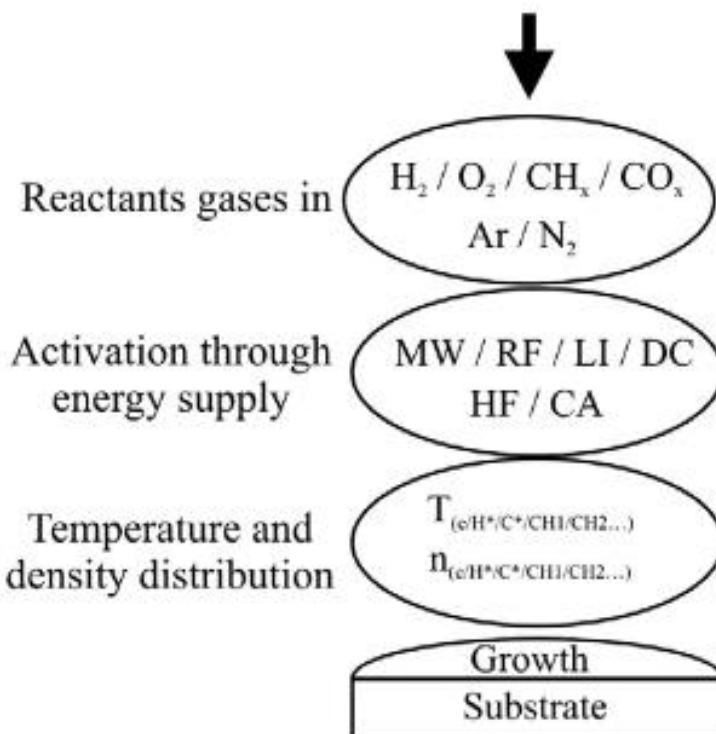


[Figure 3.1: Energy/gases involved in the CVD]^[17]

CVD is a short term for Chemical Vapor Deposition. The name speaks for itself, it's a process of chemical reaction inside a gas-phase along with deposition onto a surface of a substrate.^[17] It is a vacuum deposition method used to produce high quality, and high-performance, solid materials. The process is often used in the semiconductor industry to produce thin films in typical CVD, the wafer (substrate) is exposed to one or more volatile precursors, which react and/or decompose on the substrate surface to produce the desired deposit. Frequently, volatile by-products are also produced, which are removed by gas flow through the reaction chamber.^[18] Figure 3.1 illustrates direct and indirect adjustable parameters^[17], where the first group shows all the gasses that are utilized in the CVD procedure and the second includes different heat/energy sources for it. At the bottom there is a substrate with the NCD growth on top of it.^[17]

The most commonly used gases are methane and hydrogen (H_2). The latter is arguably the most important gas in the CVD, while methane or other gases that include carbon are only used for the said carbon's delivery. The importance comes from its purpose of removing the leftover carbon bonds from the surface of the sample. Another reason of hydrogen usage, is

its preventage of the graphite growth. Atomic hydrogen erodes the carbon atoms of graphite with sp₂ bonds faster, than the sp₃ diamond bonds.^[17] We will be utilizing the gasses CH₄ / H₂ in the ratio of 5% / 95%, respectively. Hydrogen atoms sometimes separate from the methane, leaving them at a reactive CH₂ state and if the level of hydrogen is very high, there is a slightly high probability of a chemical reaction that would result in a probable explosion.

3.2 – State of the art / equipment

The CVD chamber that we employ is the ellipsoidal resonator (Aixtron P6, MW-frequency = 2.54 Ghz, max power = 6 kW), presented on the Figure 3.2. It is not contaminated by other substances (e.g., CVD chamber that relies on boron), and on top of that is what most of the staff, where I worked on this thesis, are experienced with. Said device is equipped with the software, that outlines and runs steps of the CVD process, antenna, detector that shows the pressure inside the ellipsoid chamber before the process, the pyrometer, that observes and measures the said temperature inside of it and the many gas and pressure pipes and gas valves. Schematic of the chamber can be seen in Figure 3.3. The said ellipsoid chamber contains a sample holder, a circular thick disk made out of molybdenum with a 20x20[mm²] middle part for the samples (Figure 3.5), on the platform that can detach from it, covered with a very fragile, so-called “bell-jar”.^[17] It is a jar made of quartz, material that can withstand temperature of up to 1500°C. In pair with its thick structure, it proves to be reliable, despite the frailness. The chamber also has 2 focal points, one on the top and one in the bottom, near the place where samples would be.



[Figure 3.2: “Bell-jar” ellipsoidal CVD resonator]

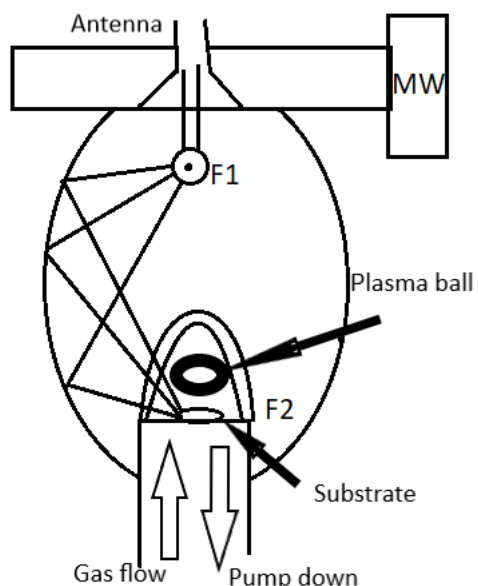


[Figure 3.3: Schematic of an ellipsoid CVD chamber, where MW is the microwave oven and F1/F2 are the focal points]

The structure also includes MW (microwave), that heats up the chamber until the plasma state is achieved inside. During the plasma state, carbon atoms get attached to the silicon nucleated surface, and they will not attach, if the silicon surface is naked because carbon does not react well with the silicon. This is why we needed the nucleation. Moreover, there is some pressure that is passed back to the MW-oven, that is named simply $P_{\text{reflected}}$. To minimize its effect and not ruin the MW equipment, we have an antenna on top of the equipment. During the plasma state, the focal point on top (F1 on Figure3.3) emits microwaves produced by the MW-oven. They reflect from the sides of the chamber's walls and pass through the quartz bell-jar as a result. Then the microwaves fall on the sample's surface with some non-zero probability, which helps in creation on the layer. The reason for the shape of an ellipsoid is reflection of the microwaves. The substrate holder slowly rotates during the act of CVD, so that the said probability is as high as possible, but unfortunately it cannot reach 100% as of now. Additionally, under the influence of plasma, O_2 turns into O_3 (Ozone), which makes it impossible for the pyrometer to detect the plasma.

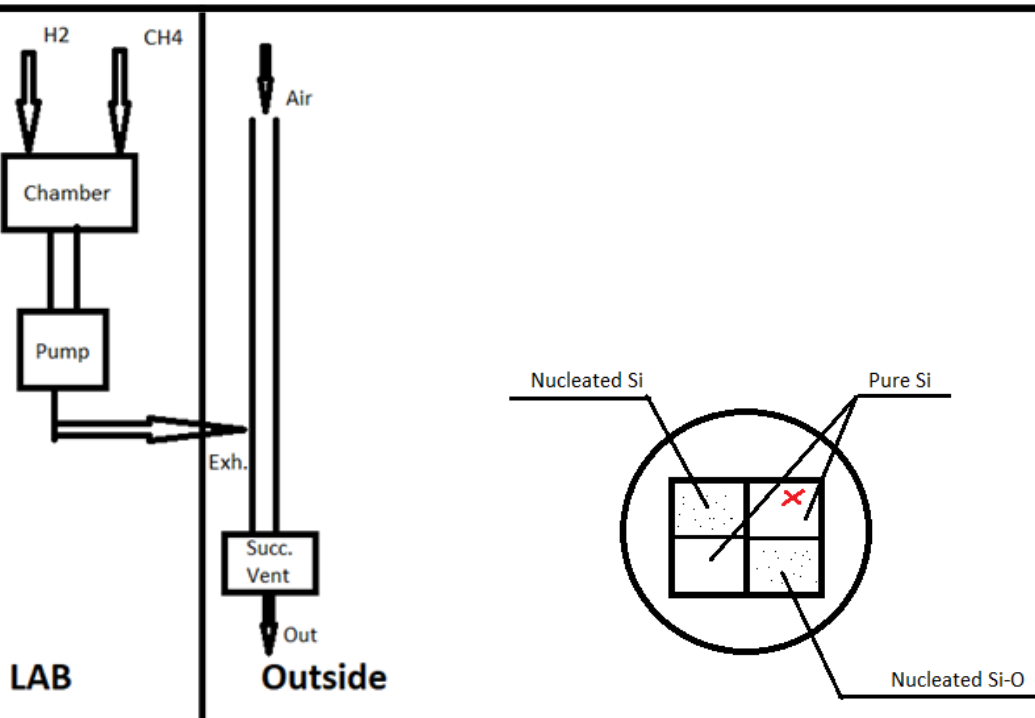


[Figure 3.4: Gas exhaust system]

[Figure 3.5: Substrate holder with the nucleated silicon samples in the middle]

There is one more pipe connected to the CVD chamber, and it is the exhaust pipe. It runs in a loop and extracts the leftover gases from inside the chamber. A lot of air is passed inside this pump and dilutes everything that passes this pump through the suction vent. The large amount of air negates H₂ proportion to 5% (Needs to be at least < 50%).

Before the experiment is started, there are some safety measures that need to be performed. First, we check the gas control panel and turn on the necessary switches. If any gasses will be detected in the room, the passing of gases will turn off automatically. The gases that will be passed in our case are CH₄(methane) and H₂(hydrogen). H₂ improves the thermo-transfer from gases to the bell-jar. Other 2 switches are “general” and “safety”. The first one turns on the ventilation system inside the room and the second introduces the exhaust tube, that is mentioned in Figure 3.4. It runs in a loop and is used to clear the chamber of leftover gases. The next part is checking the manual gas passing tubes. Since there could be a cyberattack on the equipment it is necessary to turn on the manual valves that are responsible for the two mentioned gasses and the nitrogen (Ni), since it is mentioned in the instructions.

The substrate holder is covered by the quartz bell-jar, and this is where the vacuum is created and preserved during the CVD process. It is also important to note, that under no circumstances can the CO₂ be added to the process, as NCD layer that was deposited with its addition, would not exhibit any Si-V PL peak.^[2]

3.3 – Experimental section

We deposited 6 samples of “fine” nucleation method of all three stages: 3 from Si group and 3 from O-Si group. Stage 1 has undergone deposition for 15 minutes, stage 2 for 10 minutes and stage 3 for 5, to see the differences of thickness as well as compare the Si-V PL peaks. Since the 3rd stage “fine” nucleation is the densest in terms of grains, we also deposit 2 samples of it, Si and O-Si for 5 minutes. We also used 2 of the “standard” nucleation method, one of Si and one of O-Si group. Along with the nucleated Si samples we also put the pure Si, because they dope the layer of the samples, since we need to observe the Si-V vacancies. We place 2 samples of 10x10mm nucleated Si and 10x10mm of pure Si, also 2. We mark one of them with a cross, as presented on Figure 3.5, so that we will keep track of where Si and O-Si is, as the substrate holder rotates.

The gases used are H₂, CH₄ and Ni (Nitrogen). The latter is used for the cleaning of the chamber during and after the deposition process, I assume. The CH₄ / H₂ is used in a 5% / 95% ratio, with H₂ having 300[sccm] and CH₄ 15[sccm]. SCCM is a short term for “Standard Cubic Cm per Minute” or [cm³/min]. MW power is 3[kW]. Before starting the process we wait for the detector to show 6.5E-6[mBar] or some value close to it in the same order. This is the pressure that will be preserved inside the chamber, and it is enough to create an artificial vacuum. The process of CVD has multiple steps even after the deposition is complete, so the whole process takes longer than the time required for deposition only. The pyrometer only shows a range of temperature inside the chamber, the minimal and the maximal values. Temperature during the process reach from 688°C to 800°C. As a safety measure, the temperature is written down

every 2-3 minutes from start to end of the CVD process. It is important as in very rare occasions the temperature could be lower, or in the worst case, much higher than expected. If this happens, the process should be stopped immediately!

After the deposition we also store the pure Si for later, as there might be a spontaneous growth of nanodiamond even without the nucleation, on the cross from Figure 3.5. In conclusion we are left with 6 samples of “fine” nucleation, deposited for 5, 10 and 15 minutes. 50% of it from the Si group and the rest from O-Si (the silicon samples that were put through oxygen plasma prior to nucleation). We additionally get the same amount of specimen from the “standard” method nucleation for 5, 10 and 15 minutes, and the distribution through the groups is mirrored off the “fine” method nucleation deposited samples, in other words, 3 in Si and 3 in O-Si groups. We also get 2 potentially very thin samples with Si-V color centers present as well, one from the O-Si group and one from Si, of the highest nucleation density from all the “finely” seeded silicon substrates, 3rd stage of nucleation, that were put through the CVD process for 5 minutes only.

Chapter 4

Raman, PL, AFM

38

4.1 – What is Raman spectroscopy

As light/photons get in contact with the surface of some material, there are 4 outcomes: absorption, where light is absorbed by the material; reflection; transmission, when the light passes through it without changing direction; and scattering, which means the photon/light changes its direction after passing through the material. They are influenced by the wavelength/color of the light (e.g., green light corresponds to 550 nm), and the field of study that specializes in this matter is called “Spectroscopy”.^[19] The Raman effect is an interaction process of electromagnetic waves (light) with matter in which a vibrational quantum is excited (Stokes Raman scattering) or destroyed (Anti-Stokes Raman scattering).^[20] Energy of displaced Raman photons goes up or down depending on vibrational state of the molecule, as presented on the Figure 4.1. The most common occurrence is Rayleigh when the wavelength of the scattered photon preserves its original value, and the energy of the impacted molecule stays the same as well. It is “the dispersion of electromagnetic radiation by particles that have a radius less than approximately $1/10$ the wavelength of the radiation”.^[23]

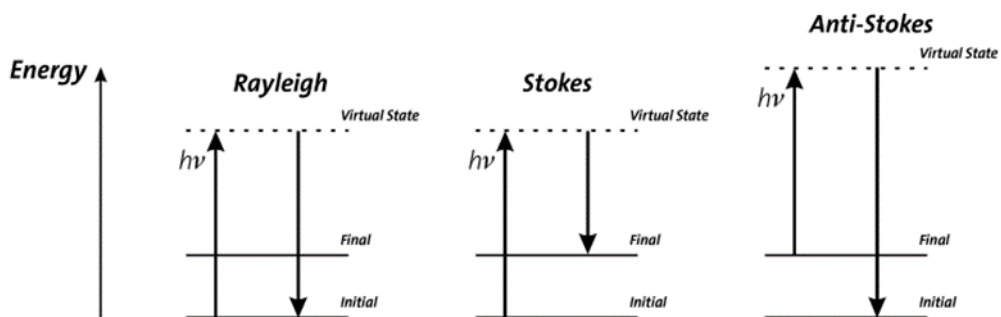


[Figure 4.1: Diagram showing influence on the energy levels by elastic (Rayleigh) and inelastic (Raman or Stokes and Anti-Stokes) spectroscopies]

Raman scattering is a bit different however, as during it there is a transfer of energy between the light/photon and the material. Upon receiving said energy from the photon, molecule of the material jumps to a higher vibrational level, photon gets scattered and loses energy, resulting to increase in wavelength, supported by their relation from the Formula 3, where W is energy, c is the speed of light, h is Planck's constant and λ is wavelength. This process is called Stokes (Raman) scattering.

$$W = \frac{hc}{\lambda} [eV] \quad (3)$$

Alternatively, anti-Stokes are the flipped Stokes, as the molecule loses energy instead of gaining it. Hence, the scattered photon loses its original wavelength. Despite Stokes and

anti-Stokes being equally likely to happen,^[19] Raman spectroscopy itself is very uncommon, occurring only in 1 of 10,000,000 photons. But there exist some methods of enhancing this effect, one of such is Raman resonance. Raman resonance is an effect that occurs when the wavelength of the laser and the electronic absorption of the molecule harmonize, and the intensity of Raman-active vibrations associated with the absorbing chromophore are enhanced by a factor of 102-104.^[21] Thus the resonance Raman technique is used for providing both structural and electronic insight into species of interest. Raman scattering from a substance(or an inert atom) can be 103 – 106 times stronger, if it is soaked up by some material, rather than inside liquid. This effect of surface enhancement is most noticeable in silver but has some effect on copper and gold as well.^[21] Raman spectroscopy can also inform of sample's chemical structure, intrinsic stress/strain, phase, levels of contamination and impurity and polymorphism. It is a type of non-destructive analysis based on how light interacts with chemical bonds in the subject material.

Raman lasers exist for this purpose, they emit light of some wavelength on top (and in cases of double-faced sample from both sides, also bottom) of the specimen and map its properties on the Raman spectrum of various ranges, so that the smaller peaks could be noticed, for example. Raman lasers very in the wavelength they utilize, usually being singular and constant in every laser, from UV light (shorter than 385nm) it can range up to almost infrared (IR) light up to 750[nm]. There are several factors for choosing excitation wavelength of the laser. Near-IR lasers lose sensitivity with their wavelength increasing. Wider wavelengths are also responsible for the low resolution of the spectrum. Excessive fluorescence emission should also be avoided, as the spectrum will be flooded with the Raman scattering signals, and the laser influence will be very prevalent in low excitation wavelength lasers, such as UV. In conclusion, there should be a balance value between the two, a “silver-lining”. Most commonly used are the near-IR or 750[nm] lasers, which avoid fluorescence entirely, and the low resolution could be easily circumvented in most cases with thorough filtering (e.g., median, average etc.). Despite this, green lasers of 532[nm] are heavily utilized in the Raman spectroscopy, for artificial materials, such as nanotubes and other nanomaterials. This wavelength provides efficient and optimal results with a relatively high resolution (depending on how high the integration time is) and avoiding fluorescence entirely.

4.2 – What is PL spectroscopy

Photoluminescence, also known as PL for short, is when light, energy or photons are directed onto the sample's surface and stimulate the emission of photon from it. It is contactless and safe method to measure material's properties, without worrying about the destruction of the latter. As light falls on the sample's surface, the surface material jumps to a higher electronic state after which it relaxes and releases energy/photons in the process. This process is called photo-excitation and it occurs in the material when photons are absorbed by it. The process of light/luminescence released from the material is hereby called photoluminescence.^[22]

Raman characterizes electronic properties of the material, so combining it with PL detection, we get access to vibrational properties as well. And the case with excitation wavelengths is no different from Raman here, as the excitation wavelength is also adjustable and also falls in the range between the weak UV (<385nm) lasers and NIR(Near-IR) (~750nm). The advantage, however, is that most PL lasers are adjustable, meaning that one laser can have all these various wavelengths accessible for analysis. However, this comes at a price, since for higher NIR luminescence, there is almost guaranteed to be influence from the laser. PL spectrum intensity only notes the values up to 2^{16} [a.u.]. Photoluminescence spectroscopy supports capability of confocal mapping, with special resolution of less than $1[\mu\text{m}]$. The photoluminescence quantum yield, also known as PLQY, related to material or a singular molecule is represented as the number of photons emitted over the total number of light (in photons) absorbed. It is a common technique in Fluorescence spectroscopy, a type of luminescence caused by molecule being excited to an electronic state by photons. After this, the molecule experiences swift thermal losses and drops to the lowest excited state. This process has distinct features of other non-radioactive, non-destructive processes, such as transfer of energy and heat loss. It is one of the most common forms of photoluminescence, other two being phosphorescence and chemiluminescence.

In practical application, photoluminescence characteristic signal of some material shows as a peak on the wavelength[nm]/intensity[a.u.] spectrum at some wavelength. For example, characteristic peak of the Si-V center appears at ~738-739[nm] of wavelength, and silicon appears as a much larger peak (in its background the Si-V peak is unnoticeable) 1,144[nm] or (1.1 eV). Such information provides knowledge about material's composition and its solid-state structure.

4.3 – What is AFM

Atomic force microscopy, also known as AFM, is an advanced technique of studying properties of materials at atomic scale. It has played a huge role in fields of science, such as physics of solid-states and molecular biology. Its origin was and still is scanning tunnelling microscopy or STM. It was invented for investigation of conductive solid material properties, their surfaces mainly. While it focuses only on the conductive materials, AFM on the other hand investigates properties of the non-conductive ones. It was invented in 1986 by G.Binning, C.F.Quate and Ch.Gerber (Binning et al., 1986). [23]

Utilizing AFM one can achieve much knowledge about the material under research, such as elastic modulus, surface potential, adhesion, electric current, surface topography and so many others. In this work we will focus on surface topography mainly as we need to measure difference in the elevation of 2 layers, the silicon and the NCD. AFM is mainly used for nanoscale research, being less reliable for large scales, such as microns (μm). This technique utilizes a probing pin at the edge of a cantilever. This pin is very small, being less than a [mm]. They are very fragile, breaking from the smallest impact and are made out of silicon or silicon nitride generally. Silicon that is highly doped and other materials with low resistance, that

AFM cantilever is made of, ensure that no electrostatic charges are concentrated on the tip apex, as they result in distortion of the AFM scans. During AFM, the cantilever tip makes slight contact with the surface it is observing, and this excites and activates the repulsive and attractive forces.^[23] During the measurement, the attractive forces pull the tip closer to the surface, while reactive forces push it away afterwards, creating a loop of the two. These forces almost act as a spring that stretches up and down and give important topographic properties about the sample, mapping points this way one by one, which is why the process is lengthy. Laser hardwired inside the microscope that runs the process sends photons, a beam on the very tip of the pin, so when it is affected by the forces, photons carry newfound data to the detector. Figure 4.2 illustrates this process:

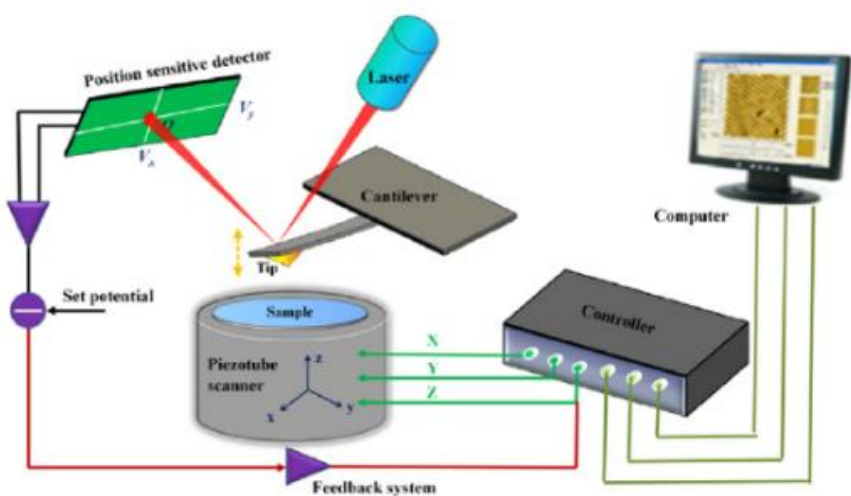


[Figure 4.2: AFM measurement example. Laser light falls on the pin, which is affected by the repulsive force and the light sends data to the detector]^[23]

The piezo tube scanner, which is the substrate under the specimen is very important, as it makes mapping of the surface in the 3D scale, possible. This measurement is less safe than Raman for example, since during contact, if the WD will be too low and the pin is close to the sample's surface, it could scratch the observable part, ruining the results. However, on the scale as small as $60 \times 60 [\mu\text{m}^2]$ these rare occurrences are not critical. There are different shapes of the cantilevers, and their variety comes in a form of spring constant k , and its range is usually from $0.01[\text{N/m}]$ to $100[\text{N/m}]$.^[23] There are two modes in AFM: the contact mode and the non-contact mode. In both of them, there is a dominant force. The former's name speaks for itself. Since it requires contact to the material's surface, the repulsive forces are prevalent there and vice-versa, the non-contact mode undergoes a lot of attractive forces. There is also another one, called tapping-mode/AC mode/intermittent-contact mode/oscillating mode, the mode we will utilize in the work. During its runtime both repulsive and attractive forces take place, hence the name. The pin is positioned closer to the sample's surface, than in non-contact mode. Cantilever undergoes resonance frequency oscillations and creates vibrations during the process. These vibrations have a constant fixed amplitude, usually small at around $1[\text{nm}]$. Amplitude this small makes attractive forces take place in the interaction between the

pin tip and the specimen. Alternatively, at large amplitudes of around 100[nm]^[23] repulsive forces will be more dominant in the interaction.

4.4 – State of the art / equipment



[Figure 4.3: Optical confocal Raman microscope]

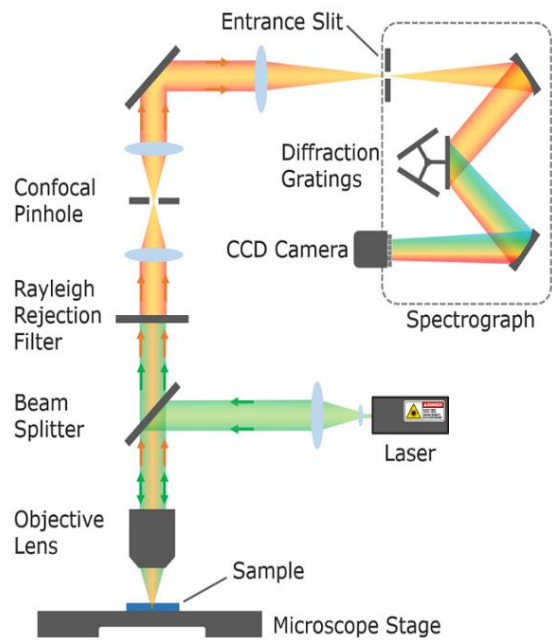


[Figure 4.4: Optical confocal Raman Microscope structure]

Optical Raman microscope (Witec alpha 300) presented on the Figure 4.3 is used for different measurements of the material properties, such as photoluminescence, Raman spectrum measurement and atomic force microscopy. It is a very complicated state-of-the-art equipment, that has 4 lenses of different magnification: the 20x lens, used for focusing and is unique for being the only magnification utilized for AFM easurement; the 10x lens, rarely used, I think for moving through the surface of samples with larger area; 50x lens; and 100x lens, used for PL and Raman spectrum analysis, very hugh magnification with WD down to a few mm. There is a camera that takes the image from the lens and shows it in the software, "Witec Control 5" in real time. Joystick sticks are used to move up and down to find the focus of the sample's surface. The switches for turning the light off that passes the image to the camera as well as the camera itself are present.

The platform is capable of producing normal scans of the sample's surface and various spectra's, such as Raman and PL as the most utilized ones. It can generate spectra and images from the samples that reach diffraction limit of 1[μm]. Research grade optical Raman microscope is coupled with spectrometer/detector and three excitation lasers. The first one is the laser for Raman spectra measurement. It has a power control switch, and its power can

go up to 7[mW] and higher, but an energy this high might damage the sample so we use a lower one, ~4[μ W]. After booting up, the laser must reside for 30 minutes before it can be utilized, as it undergoes calibrations each time. The excitation wavelength of the laser is always 532[nm], which corresponds to green light, as the green light's spectrum is around 550[nm]. Second laser is for photoluminescence measurements. It is controlled from the software "Witec Control 5", that can change such features as bandwidth, excitation wavelength, power of the laser and so on. Power of the laser is changed in %, the most common being 15%, 75% and 50%, but the multimeter also shows units in [W] or rather [μ W], as its power works the same way as the Raman laser. Its wavelength can be controlled, the bottom limit is 400[nm] and the upper is 700[nm]. The device also has a place for the optical filter, which is used for PL measurements only, as there are multiple wavelength's options, and the laser influence could be noticed without it very clearly. Even with a filter of 715[nm] we can still reach a signal of 2^{16} [a.u.] in intensity units, which makes the data unreadable and unreliable, still being able to zoom on the important part, however. The last is laser used for AFM measurements inside the Raman microscope itself. It has a wavelength of up to 1300[nm] and the power could reach [mW] or even [W]. Laser's influence could be turned on and off at any moment, as there are switches controlling the flow of each individual laser.

The Raman microscope structure stands on the spring induced calibration platform (TS-150 Tables Stable), that upon turning on and device experiencing any tilting will automatically begin the calibration process to position the device straight and level it horizontally as well. It is very useful for the AFM measurement for example, where the surface topography could be messed up because of slopes. Figure 4.4 shows the structure of the Raman microscope and additionally the spectrograph. Light inside the device is sent from the laser and reflected by mirror onto the sample, after which it travels upwards, through the Rayleigh rejection filter, that cannot be removed, hitting another mirror, and sending the material properties through diffraction gratings to the CCD (Charged couple device) camera, or the detector, in a form of light. The spectrum of the sample and its properties is achieved this way.



[Figure 4.5: AFM microscope Dimension Icon Bruke]

Another device used is AFM microscope Dimension Icon Bruke in FZU (Figure 4.5), that “delivers unmatched large-sample resolution with open loop noise level, reduced noise floor and <200[pm] drift rates”^[24] as well as showing the RMS on nucleated surface. Although the confocal Raman microscope is multifunctional and includes AFM as well, it underdelivers when compared to this one. Icon Bruke AFM microscope’s structure allows it to not be influenced by noise or vibrations, instead of the calibration table, the device has a foundation in the building that keeps it from tilting, very efficiently. Its microscope works quite like the one we used in SEM, moving freely through the circular observation substrate, which is way more than enough space for the samples of 5x10[mm]. its radius reaches size of ~20[cm] or larger. In technical properties, its objective lens can measure in the scale/range of 90[μm]. Also has <200[pm] drift rates.

4.5 – Experimental part

Experimental part will consist of Raman followed by AFM and concluding with PL measurements including drop-casting the NCD surface. It will not necessarily be in this order, as sometimes measurements are performed due to other measurements (e.g., PL characteristics unpredictable, so required to do AFM).

First of all, we perform the Raman measurement on the state-of-the-art confocal Raman microscope. After turning on the “Witec Control 5” software, we simultaneously turn on the microscope itself. For the Raman measurement we use a green light laser, with a constant excitation wavelength of 532[nm]. We use it under the power of 4-4.5[μW], which is observed by the multimeter. We only check the value on the multimeter when absolutely necessary since it blocks the stream of photons. In the software, under the “configurations” we choose Raman spectroscopy [1/cm], as Raman shift will be depicted in these units, which indicates that we will be measuring Raman. There are also other options such as AFM AC and PL [1/nm] that we will utilize later. We then set important parameters for the Raman measurement. First we did Raman of the “standard” method nucleated samples that have undergone CVD for 5, 10 and 15 minutes. Central Raman shift was set to 1600 [1/cm] at first and grating, which is the scale or range of it, to the mode always used for the Raman measurements, G3, as it is the smallest scale, being less influenced by other peaks of non-NCD material properties. After we got a straight line of the spectrum at the range of 1100-2000 [1/cm] followed by a large upwards slope, we decide to increase the integration time to 5[s]. Since the slope was at 2000 and further it could not have been a NCD characteristic, which is at the x-value of 1339[1/cm]. As references in the article of Stepan Stehlik about creation of thin nanodiamond layers,^[2] we want a range between 1300[1/cm] and 1650[1/cm], but with this device it will not be possible, unless we zoom in, which compresses the data slightly, so we decide not to do that and leave the range as it is, at 1100-2200[1/cm]. We tried to change power of the laser from 4[μW] to 7.08[μW], increased number of accumulations to 50[-] and left the integration time at 5[s] and finally got the desired peak at 1339[1/cm]. There is also an option for scan of the observable NCD surface, but this is time consuming and not important for the

goal of the work, so we disregard it, only observing the spectrum of the sample from Raman analysis. The signal achieved is jumbled and has much noise and many peaks, which are artificial peaks, created by the laser itself. This is because the microscope is very sensitive to any significant vibrations, noise and sometimes even light. Thankfully, during the laser shooting, the substrate area is covered with a protective box, for safety measures, so light does not impact it enough to take effect. However, we will never get a perfect signal, so we keep the results and “fix” them. In order to “fix” the spectrum we apply a filter that is most suitable. Usually, the most common method is to use the “Average” filtering, but when there are peaks, this method is obsolete, as it will not filter, seeing them as a part of the material properties. For this issue we have a “Median” filter, that easily mutes all the peaks on the spectrum. From all 3 NCD deposited samples of the “standard” nucleation on top of the silicon substrate, we take 3 spots in 3 parts of the specimen, divided by the cross section made during the nucleation periods. 2 of them were taken far from the scratch and one right next to it. The signal is very diverse in all 3 spots, and this is true for all the “standard” method nucleated samples, that were later deposited for 5, 10 and 15 minutes. This further supports the claim of inhomogeneity of the NCD film surface after (and before) the CVD. The NCD Raman peak at 1339[1/cm] was noticed to be the strongest in the 2nd spot, not next to the scratch. Then we perform the same measurements, for the “standard” method nucleated and later deposited sampled, but of O-Si group, samples that were oxygen terminated prior to the nucleation treatment. Parameters stay the same, namely grating, power, integration time, number of accumulations, excitation wavelength of the laser. Second set are the samples that have undergone CVD for 5, 10 and 15 minutes after the special “fine” method nucleation, as well as those from the Si group that we measured. Raman spectrum of the thicker samples(15 minutes CVD) displays a base intensity, that is ~11.1[%] larger in the case of O-Si group and ~10[%] larger in the case of Si group, than that of thinner (5, 10 minutes deposition) samples.

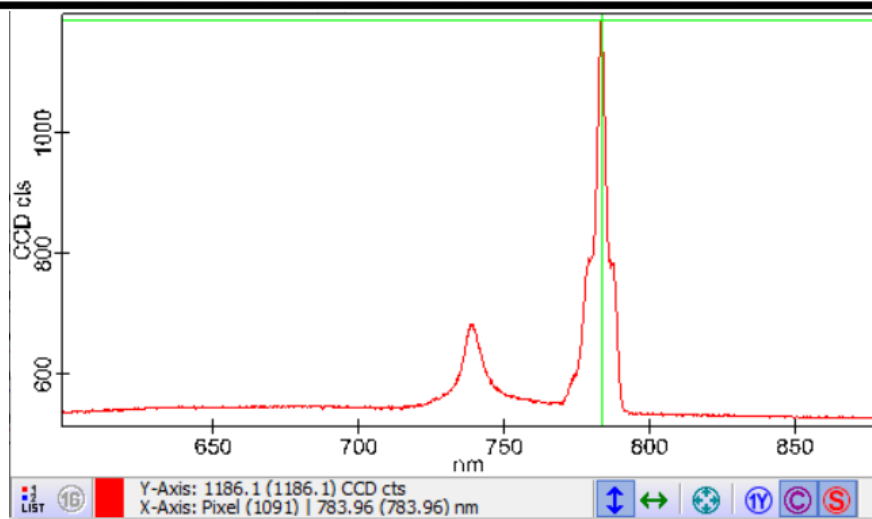


[Figure 4.6: PL Si-V peak of a thick (>150 nm) NCD deposited sample (Low peak) and the influence of the laser (High peak)]

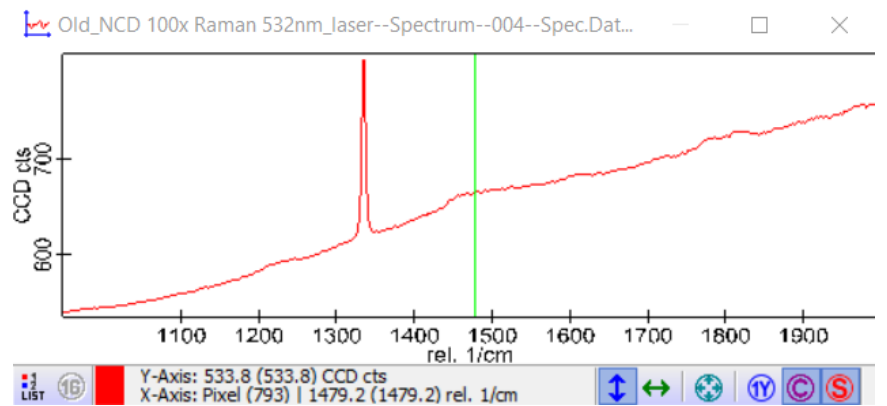


[Figure 4.7: Raman spectra of a thick (>150nm) NCD sample ($\lambda_{exc} = 532\text{nm}$)]

After the Raman spectrum analysis, we perform PL on the same “fine” NCD layer samples. We first set the integration time to 0.5[s] and the number of accumulations to 15[-]. Laser wavelength was set to 469.2[nm], corresponding to blue light, as we need any wavelength below 730[nm] (which the device isn’t capable of detecting regardless). Power was first set to 70[%], but later changed to 15[%], so the final power of PL laser is 4.08[μW]. Bandwidth is set to 1.0[nm] and we do not change this value for the PL measurements. We were continuously getting the PL Si-V peak at 748[nm], which we thought was a spectral shift in the device. Throughout the measurements, we realized that the PL does not show the correct Si-V peak, as it appears even on the pure silicon in the same place (748nm). This value is not an Si-V peak (738-739nm), but at the time we thought, that it is the shift in the system. We noticed it when we were measuring PL for the same deposited sample of NCD, and the intensity changed over time without any influences. So, we took an NCD layered silicon sample of a very high thickness (>150nm), which is supported by the large Raman peak, characteristic to NCD (Figure 4.6). We made PL measurements for it ($P_{laser} = 15\%$ (4.05mW), λ_{exc} (excitation wavelength) = 469.2nm, # of accumulations = 15, integration time = 30s, laser filter = 715nm). Then we noticed that the Si-V peak appears, but it is very mute in regard to the larger peak, that is either the laser interference or the material properties. Since the peak appears on any sample, I believe it is the first option. The peak is also so incredibly large (~1180 a.u.), that the Si-V peak next to it is small (~680 a.u.), that the filtering of the signal is not necessary (Figure 4.5).

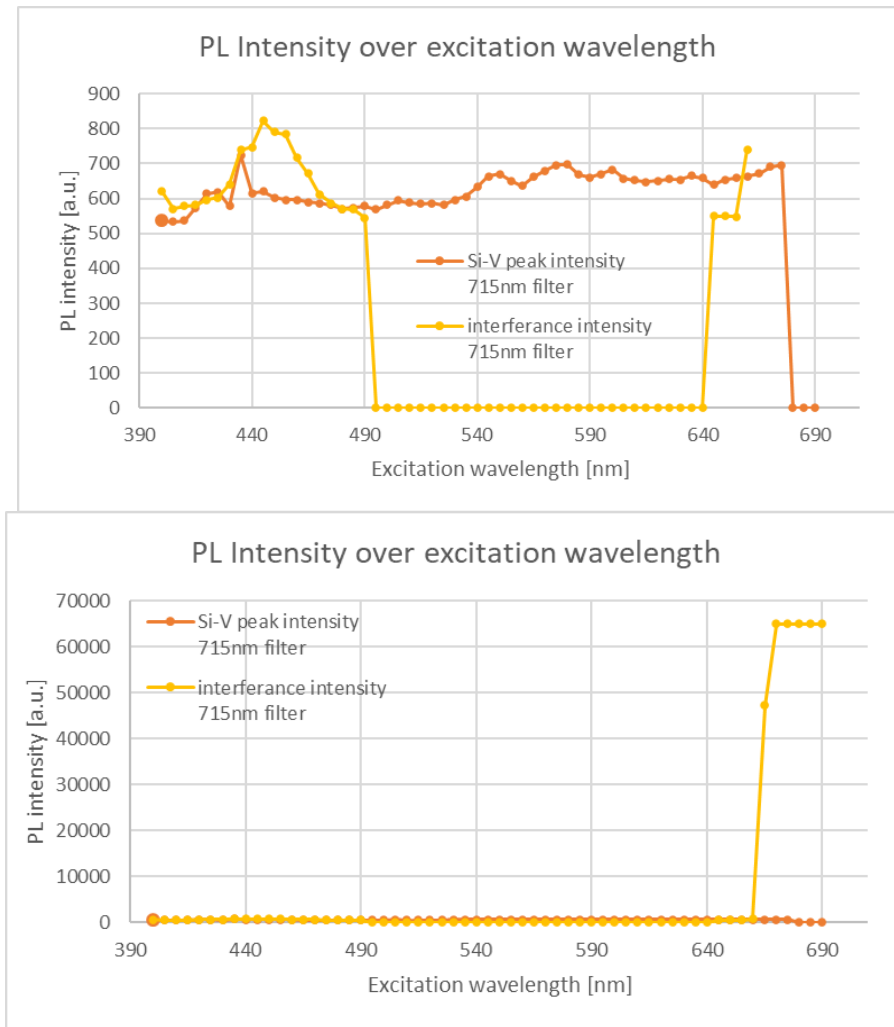


[Figure 4.8: PL intensity of the NCD deposited thick (>150nm) sample over the λ_{exc} of the laser showing Si-V and laser interference peaks from 400nm to 700nm with a 5nm step]

As a result, for the same sample we measured PL in the same spot, from 400[nm] to 700[nm] with a [5nm] step, in order to spot the highest Si-V peak and the lowest laser influence. We also increased the integration time, as this would allow us to see Si-V peak on a thinner NCD layered silicon samples. Parameters are the same, except for the excitation wavelength (λ_{exc}): $P_{laser} = 15\%$ (4.05mW), # of accumulations = 15, integration time = 30s, laser filter = 715nm. The graph of laser's λ_{exc} relation to the Si-V peak it shown on the Figure 4.7. The Si-V peak in this relation is represented by orange graph, while the interference of the laser is marked by yellow. At the 400-430nm there are some interfering peaks. At 435-490nm and at 435nm especially, the peaks are on the 738nm or close to it, interfering too much to see the Si-V peak. At 495-640nm there are no interfering peaks and the local maximum for that range is 575-580nm with 696-697 units of intensity. At 645-700nm the peaks interfering become too large to see anything (Figure 4.7, bottom graph), as the intensity value far exceeds the upper limit that the device can read (65,536 a.u. or 2^{16} a.u.) and although zooming helps on this sample, I doubt it will be precise on the ones with smaller NCD layer. The local maxima overall are at

690nm being 1350 units of intensity [a.u.], but it is hard to note due to large interfering peaks. I chose 575nm for my measurements of PL.

We also increased the integration time, until we could see a PL peak on the thinnest samples. Although this resulted in failure, as no Si-V peak could be distinguished even at 4[hours] (Figure 4.8). Additionally, integration time is proportional to the quantity of spikes we can get on the spectra. Spikes are the artificial sudden peak, that in most cases only appear on one point of the x-axis and have a very high intensity.

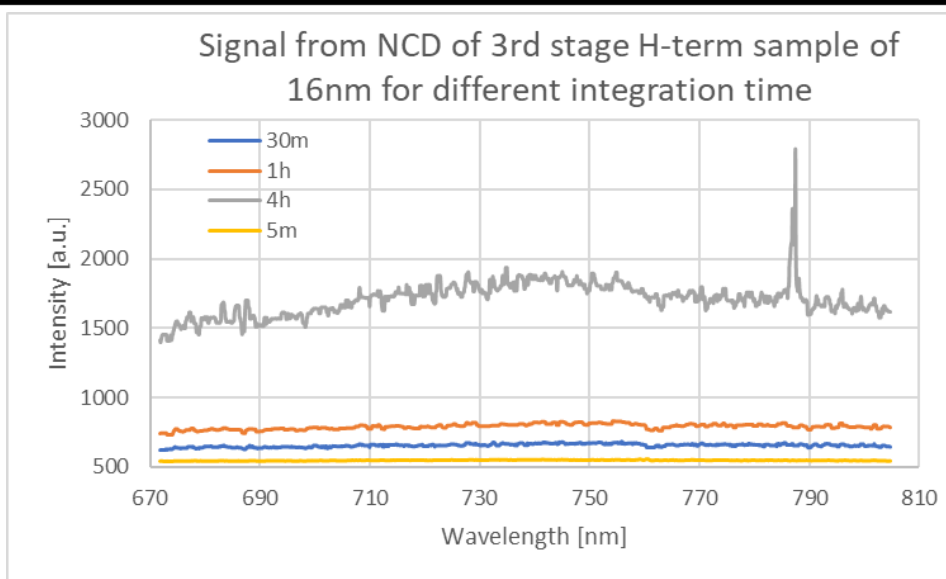


[Figure 4.9: PL spectra of 16[nm] H-term(hydrogenated) NCD layer under four different integration times]

They are easily filtered by the Median filter in “Witec Control 5” software, that is also part of the microscope. Referring to the Figure 4.8 one more time, it seems that as the integration time increases, the basis of the signal rises along with it. Unfortunately, 4 hours is not only too long, but also cannot be filtered properly, and there is no Si-V characteristics that can be noticed between 30[minutes], 1[hour] and 5[minutes], so the most optimal solution that I chose is to stick with integration time of 5 minutes. We do PL measurements of the following samples:

- 1) 2 samples of 16[nm] NCD layer, that were 3rd stage nucleated prior to deposition. CVD took 5[minutes].
- 2) 6 samples deposited from the “fine” nucleation. Deposited NCD layer from the 1st, 2nd, and 3rd stages on nucleation respectfully.
- 3) 6 samples deposited from the “standard” method nucleation for 5, 10 and 15 minutes.

From all 3 groups, there were 2 samples of the same thickness and there is a reason for that. We want to see the differences between hydrogenated and oxygenated samples after the deposition, as oxygenated samples have shown higher Si-V properties on the spectra.^[2] set

of samples was oxygenated for 4[minutes] under the power of 100[W] and the other was already hydrogenated from the CVD process, as it uses a lot of H₂.

Before we can measure PL characteristics further, we must find out the thickness of the 3 nucleated samples and observe samples of 2nd and 3rd stages of nucleation. So, we conduct the AFM measurements. We place the sample on a plastic desk and position it under the lens of the microscope, on the substrate holder. After switching the lens to 20x magnification, goes focusing on the sample. Moving to 3000-4000 in WD is followed by connection of the pin. A very tiny silicon pin on circular substrate of another material is placed on the cantilever holder. Substrate with the tip of AC AFM and KPFM was used, with 5[um] and 10[um] in length and tip frequency of 285[kHz]. After carefully positioning it, so that the pin is visible on the camera, we control it through the software, playing with the contrast and brightness options and moving the tip on the image. We then set probe position and put it under the laser light. The laser light should be close to the edge of the tip, which is positioned judging by the sum value. It should not be minimal or too high, otherwise the circle in diode alignment to the middle of the cross(next step) will move diagonally when the right way is horizontally/vertically only. I've had multiple issue with this step, as the laser light in the software was not circular. After writing all the necessary parameters in the software: Initial-final f = 50[kHz], amplitude = ~1.0-1.1[V], driving amplitude (not constant, dependent on the amplitude), the phase is set to ~30° manually on the special pin representing spectrum, setpoint = 0.25[V], P-gain = 10%, I-gain = 6%, points/line and lines/image = 256[-] for both cases with observable geometry of 70x70[um] and time/line = 2.56[s] with minimal time for retrace = 0.5[s].The process takes 30[minutes] – 1[hour] with these parameters and in conclusion we get 4 scans: Amplitude, Phase, Topography and Feedback, with 2 copies of each: forward and backward.

Since we want to observe thickness of the NCD layer, we only utilize the topography forward scan. This is the point where the scratch we made comes into play. By measuring topography of the NCD surface and the scratch together, we can make a line scan and calculate sample's thickness. As it turned out, the bare AFM topography is not enough, as when doing the line scan, we noticed that the surface is sloping, and the thickness cannot be measured reliably. Moreover, without any filters, the total thickness of a sample will not be dependable, as the NCD grains right on the edges before the scratch are more aggregated. In order to fix this issue, we use a program Gwyddion (ver. 2.61). Gwyddion is an open source and free to use modular program, covered by the GNU (General Public License) that specialized on SPM (scanning probe microscopy) visualization of data and its analysis, primarily the analysis of topography that includes a difference in heights, obtained by SPM, AFM, MFM, STM, SNOM/NSOM. It supports a lot of SPM data formats, including the one used in the "Witec Control 5" software (.WIP). It provides a large number of data processing functions, such as data correction, filtering, leveling, grain masking functions, statistical characterization, line

scans and other important features. The application also provides with a variety of experimental and unusual data processing methods, that could be very handy. [25]

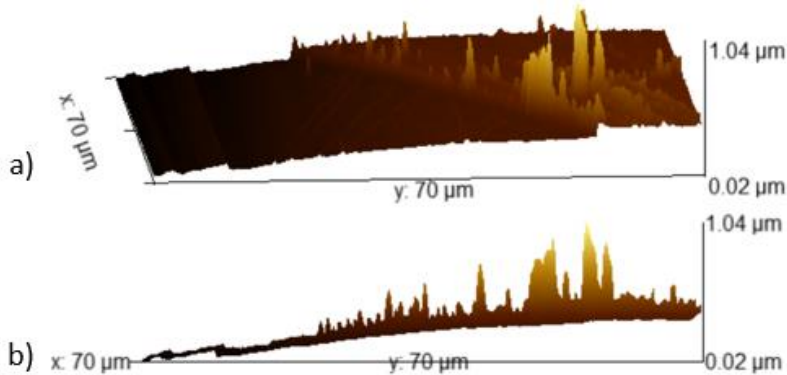


[Figure 4.10: Raw tilted 3D map of the 1st stage “fine” nucleated and later deposited for 15 minutes NCD surface on top of silicon topography. a) view from the top; b) view from the side]

When we boot up the program and choose the file with AFM measurements, we use the “info -> show data browser” function and choose the topography forward scan. Looking at its 3D map we verify that the image is, in fact, sloped (Figure 4.9). Through various Gwyddion filters this issue is easily fixed. We first use the “Median” filter under the “Allign rows using various methods” function and shift the minimum data to 0, as otherwise the minimum will be another value, e.g., 0.02[um] on Figure 4.9. Then we “level data by fitting a plane through 3 points” under the “tools” section, that we choose manually. I chose to use this function on the silicon layer/the scratched surface, because using the NCD layer would make it more homogenous, which will create relatively faulty data, while the silicon layer experiences minimal changes.

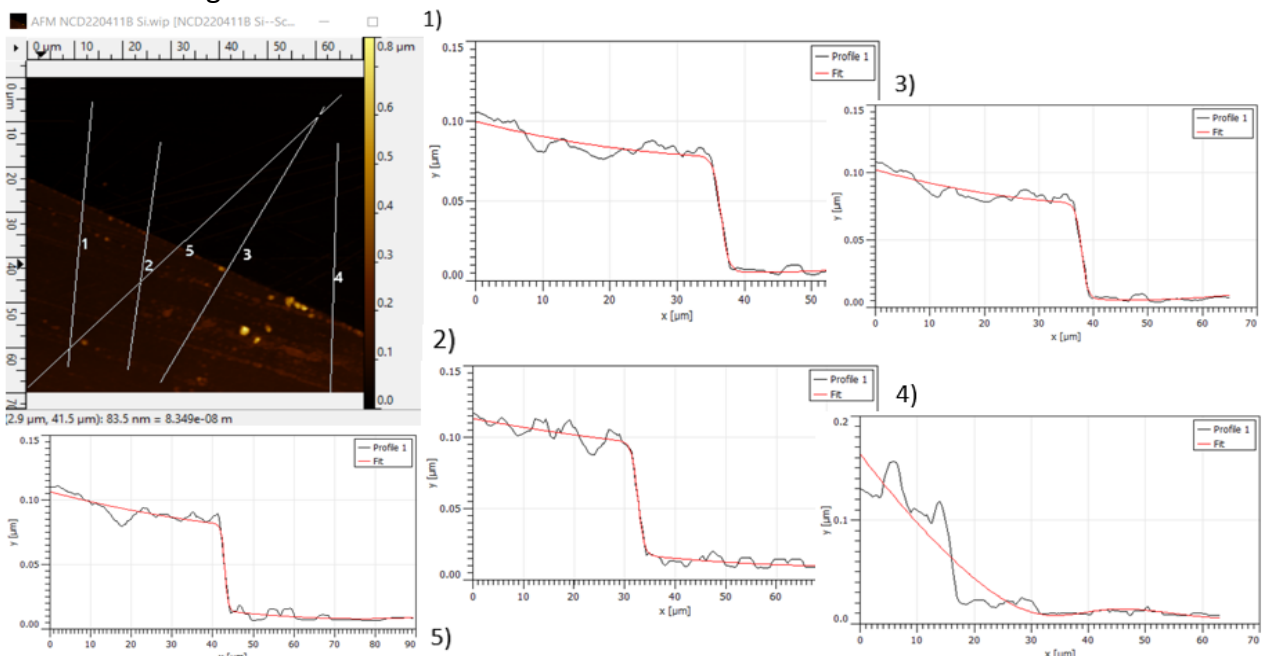


[Figure 4.11: 5 line scans of filtered topography of the 1st stage “fine” nucleation deposited NCD surface (15 minutes in CVD) on top of silicon, indicated by respective numbers]

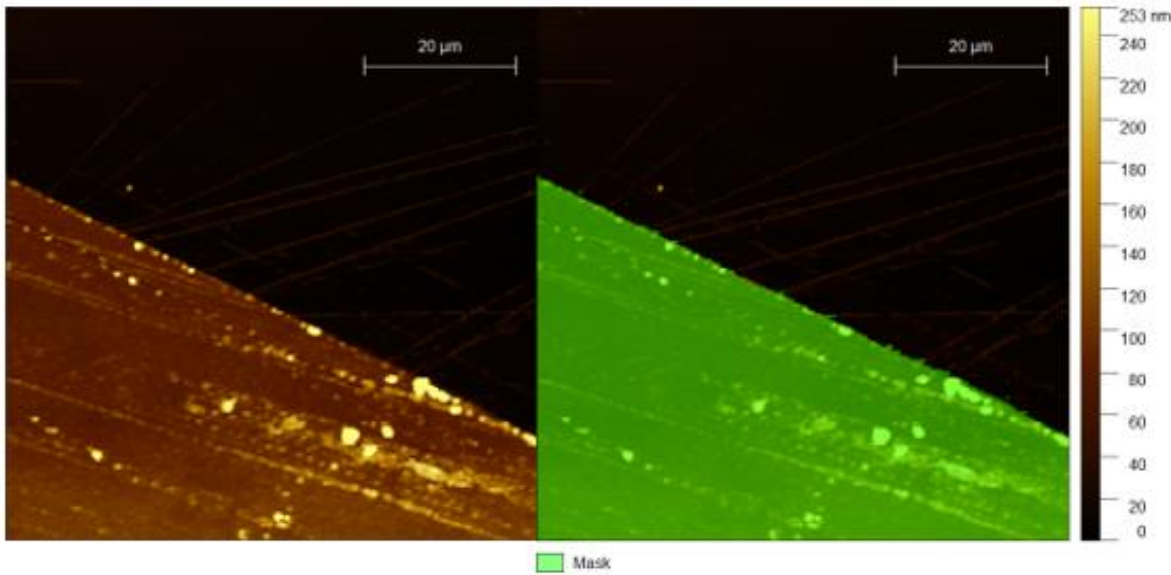


[Figure 4.12: Filtered AFM topography of the 1st stage “fine” nucleation deposited NCD surface (15 minutes in CVD) on top of silicon, original and masked]

Usually after this the 3D map straightens, but there is one optional step if that is not the case. We utilize “Polynomial” filter of lower degree (e.g., 1-2; maximum is 5) under the “align rows” data process. We can increase the brightness/contrast, to outline the grains and make the difference in layers more visible, however this is optional as well. For the final step, we shift the minimum value data to zero and achieve the filtered topography, that we can now use to measure NCD layer thickness. After the process is finished, we can use the “Extract profiles using arbitrary lines” function, which essentially makes line scans. I will use the 1st stage nucleation sample, deposited for 15 minutes, as an example. Line scans show us the spectra of the topography with width in [um] as an x-axis and length as a y-axis, also in [um], as it is presented on the Figure 4.10. To measure the thickness on the line scan I used the fit function, accessible from “Right click on the line scan -> Measure features -> Fit function”. I used the parabolic step, as it outlines the elevation difference best. However, this method is unreliable. Result shows a large amount of error, in the case of this sample, the result is: $h_{\text{average}} = 73.42[\text{nm}] \pm 58.5[\text{nm}]$ (estimated error) as an average from 5-line scans. Error is more than 50% of the thickness value itself! One more point touches the weird parabolic step fit on the Figure 5.10, in the 4th line scan. Luckily we have another method. There is a “Mark grains by threshold” function in Gwyddion that allows to mask/unmask layers by their y-value (thickness) and remove/add the mask manually if required. Using this, we can get the average height of the masked and unmasked layer. Using topography of the same sample, deposited for 15 minutes, we mark grains by the minimal threshold of 3.82[%] (or 28.82nm), which includes a small part of the silicon layer as well, so we remove it manually. Finally, by “statistical quantites” function in the “tools” section, we can measure the masked/unmasked layer, and subtract them. For this sample, average height of the masked layer (NCD) is 102.9[nm] and for unmasked (silicon) is 11.0[nm], which concludes the average thickness of the NCD layer

value as 91.9[nm]. We round it up to 92[nm]. On the figure 4.12 leveled topographies of the 1st, 2nd, and 3rd stages of nucleation NCD deposited for 5, 10 and 15 minutes respectively. In conclusion, we found thickness using AFM and Gwyddion data analysis to find thickness of these samples:

Thickness of 1st stage nucleated silicon substrate CVD-ed for 15[min] = ~92[nm]

Thickness of 2nd stage nucleated silicon substrate CVD-ed for 10[min] = ~32[nm]

Thickness of 3rd stage nucleated silicon substrate CVD-ed for 5[min] = ~25[nm]

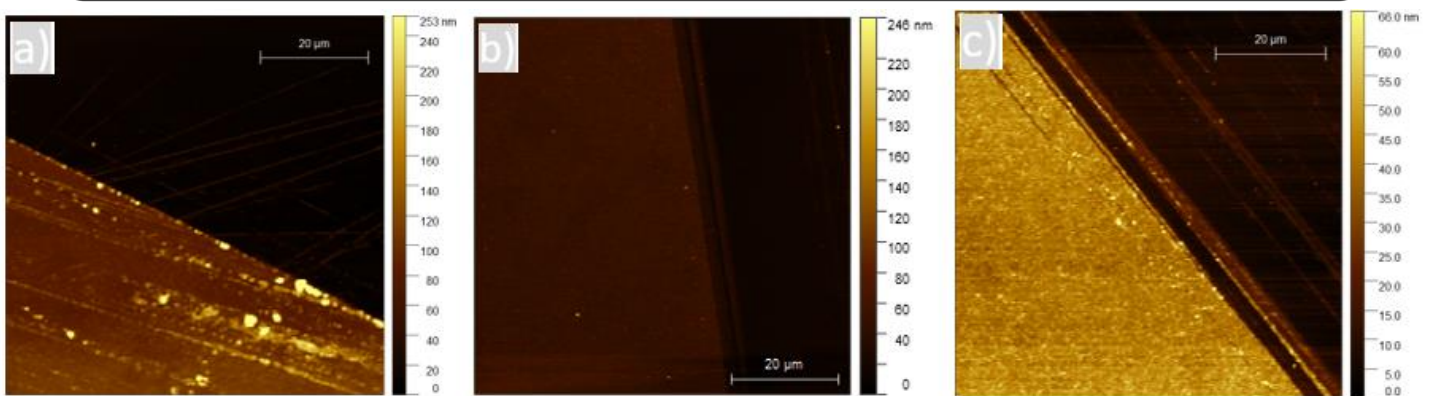


[Figure 4.13: Filtered & leveled AFM of deposited Si substrate samples of 3 “fine” nucleation stages: a) 1st stage 15[min] CVD; b) 2nd stage 10[min] CVD; c) 3rd stage 5[min] CVD]

We then also measured AFM on the potentially thin NCD layer samples achieved from the 3rd stage “fine” nucleation and they proved to be reliable, as both exhibited NCD layer thickness of only 16[nm].

The second step of AFM is to find thickness of grains in various spots of the nucleated 2nd and 3rd stages samples. The Raman optical microscope is not suitable to measure on the scale this low (2-5nm²) and for higher scale the height of grains is unnoticeable. For this purpose we utilize a different AFM measuring machinery, AFM microscope Dimension Icon Bruke in FZU under the PFQNM mode using already utilized before SNL-A ultrasharp cantilever. Results have shown, that the average grains of the samples is ~4[nm] and we used this in the earlier stages of SEM, for choosing the most optimal density for all the nucleated samples. 200×200 nm² area were measured. Two spots were measured on all samples with following parameters: Image size 1024×1024 px², scanning speed=0.13 Hz, Force threshold=100 pN, gain=1, Peak force amplitude=20 nm. Some very large grains were present as well, meaning the method of nucleation does not guarantee absolutely perfect results. The topography as well as spectrum of the line scan are shown in Figure 4.13. RMS for the 2nd stage nucleated sample is 2.48[nm] and for the 3rd stage is 3.19[nm].

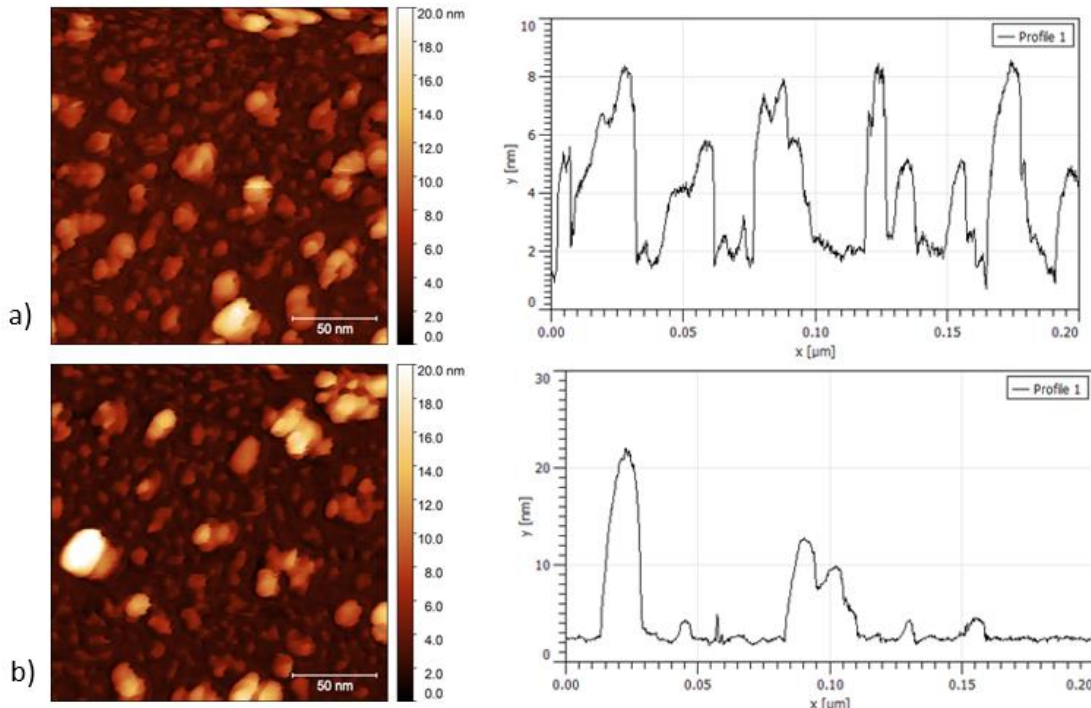


[Figure 4.14: AFM topography of nucleated “fine” method samples of 2nd and 3rd stages with their respective line scans a) 2nd stage nucleation topography/line scan; b) 3rd stage nucleation topography/line scan]

Having found the thickness of “fine” NCD layered silicon substrates, I will now refer to these samples according to their respective values. There were 2 sets of samples prior to deposition, the ones that have undergone oxygen plasma, or O-Si and the ones that have not or just Si. I did not use the second set of samples to find the thickness, as there are no differences in them after the deposition, and this is clearly illustrated by the Figure 4.13, where integration time was set to 3[s], so their PL peaks have lower intensity, but share the same height. Distinguishing the samples in these 2 groups is obsolete on this stage of work.

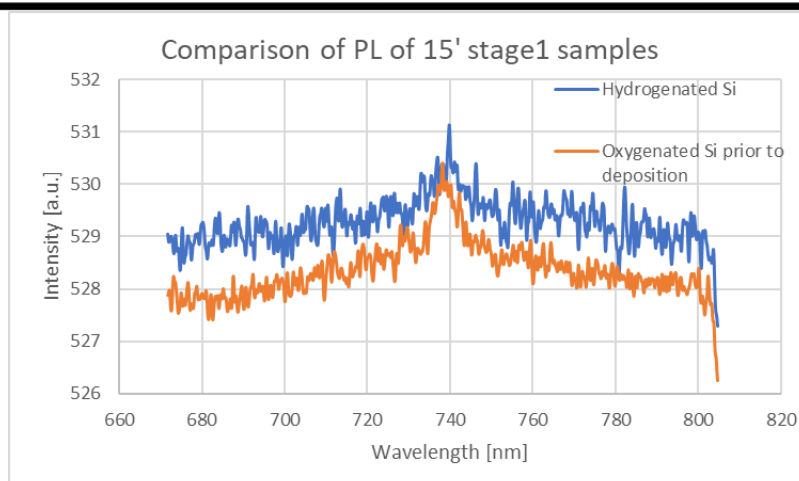


[Figure 4.15: PL analysis Si-V peak spectra comparison of the Si and O-Si(Oxygenated during the nucleation stage) groups of the 92[nm] NCD layered samples]

Next step is performing PL on the “fine” NCD layer samples, to detect the Si-V peaks. Measurements have been done multiple times throughout the work, with the most optimal being chosen. The parameters for this optimal measurement are: integration time = 3[min] or 120[s] (decided from Figure 4.9), number of accumulations = 1[-], magnification of objective lens = 100x with the scale of 10[μm]. Excitation wavelength of the laser was decided to be 575[nm] and its power set to 15%. Half of the samples were put under the oxygen plasma treatment, as it theoretically increases the Si-V peak, which we also observe under the PL analysis. For the reference we also measure PL of pure silicon.

After this we drop-cast the samples with BSA and FBS. We drop cast two samples of 32[nm] thickness with solutions of 30 [mg/ml] made in 2019(the latest that was available). Both samples were observed: NCD under oxygen plasma treatment or O-NCD/O-term NCD and NCD under hydrogen treatment or H-NCD/H-term NCD. Because CVD process includes a lot of hydrogen, it was decided to count the samples out of the CVD as hydrogenated. We make sure to drop cast both chemicals on the same NCD layer, without mixing them up. We use a micropipette (CAPP Bravo 0.5-10ml capacity) and take 1[ml] of chemicals separately, slowly drop cast on the surface and distribute by the micropipette tip. After each distribution we wash the tip with 2ml of water, so the proteins don't mix up. Aside from the “fine” NCD layer samples of 25[nm], 32[nm] and 92[nm] we drop-cast the non-shining NCD samples, or samples that display no Si-V properties and the pure Si. PL analysis parameters are the same, with change of integration time from 3 minutes to 5 minutes: integration time = 5[min] or 300[s], number of accumulations = 1[-], magnification of objective lens = 100x with the scale of 10[μm]. Excitation wavelength of the laser was decided to be 575[nm] and its power set to 15%. The chemical properties on top of the NCD surface were measured and the NCD surface itself were remeasured at integration time of 5[min] or 300[s].

Finally, we performed AFM of the drop-cast on top of the 16[nm] samples, to find its thickness. As the surface is inhomogeneous, we took 4 spots on the drop-cast. 2 from the edges and 2 from the middle. The middle part's thickness was found by scratching the surface there very lightly, so that the NCD layer remains.

Chapter 5

Conclusion and possible suggestions

55

5.1 – Summary of thesis and fulfillment of the targets

The grown silicon samples with a “fine” method had a nucleation density of the power 10^{11} as measured from the summary of chapter 2. Comparing this to nucleation density of the conventional or “standard” method nucleated samples, that had a density of $9.0 \times 10^6 [\text{cm}^{-2}]$, we can see why the method used is much better and optimal for further deposition and thin NCD layer creation. Even the thickest samples (92nm) of the “fine” nucleation, which was a result of 15 minutes deposition had a density of 10^{11} and $10^{10} [\text{cm}^{-2}]$. The “fine” nucleation method was done similar and in accordance with the article of Stepan Stehlik about ultrathin nanodiamond film of 2[nm] nucleation thickness.^[2] Although, nucleated surface of the sample appears to be slightly inhomogeneous, with large grains of 20-30[nm], but on very rare occasions, as presented on the Figure 4.14. Despite these unfortunate formalities, the average size of seeding is 4[nm] and the nucleation density is thus highest for the 3rd stage of nucleation and the 2nd stage, but only on silicon sample that was not oxygen terminated prior to nucleation. 3rd stage nucleation then displays the following densities of grains per area(Table 2 on page 30 and Figure 2.12 on page 32): Si group 2nd stage has $\sim 3.11 \times 10^{11} [\text{cm}^{-2}]$; Si and O-Si groups of 3rd stage have $2.79 \times 10^{11} [\text{cm}^{-2}]$ and $3.20 \times 10^{11} [\text{cm}^{-2}]$, respectively. In comparison to the 1st stage density, which is $1.18 \times 10^{11} [\text{cm}^{-2}]$ for Si and $7.92 \times 10^{10} [\text{cm}^{-2}]$ for O-Si, this is an optimal density, that potentially results in thin NCD layers from the CVD process.

Layer of the silicon sample of the 1st stage “fine” nucleation that was deposited for 15 minutes is 92[nm] in thickness, much more than the threshold of 50[nm]. There are multiple factors to this result. The deposition time of 15 minutes is significant enough for the layer to become thick. The nucleation influenced this as well, as in the first stage nucleation, grains are agglomerated, large and the density of the layer is lower, which is supported by SEM observations. When NCD layer grows, the grains don’t increase in width and length alone, they also gain height. Their radius increases, the same way droplets of water act when combined. The reason for this high thickness is low density of the nucleated grains, their major size and high time of the CVD process (15minutes).

Layers of the silicon substrates that were 2nd and 3rd stage nucleated and then deposited for 10 and 5 minutes, respectively, show sufficient thicknesses of 32[nm] and 25[nm], which falls in the category that we desired, as they are below 50[nm]. The results are great, as both 2nd and 3rd stages displayed great nucleation density of 3.00×10^{11} . These samples would show greater differences in PL peaks of the layer and the drop-cast unfrozen chemical (e.g., BSA) on top of it.

From the Raman analysis we can see that it is indeed an NCD layer, since an NCD layer displays a characteristic peak at $1339 [\text{cm}^{-1}]$ on the Raman spectrum. Although this peak is

not seen clearly on the samples with smaller layer, the one that was deposited for 15 minutes displays it perfectly under the same conditions, for both oxygenated and hydrogenated groups. The results are demonstrated in the Figure 5.1.

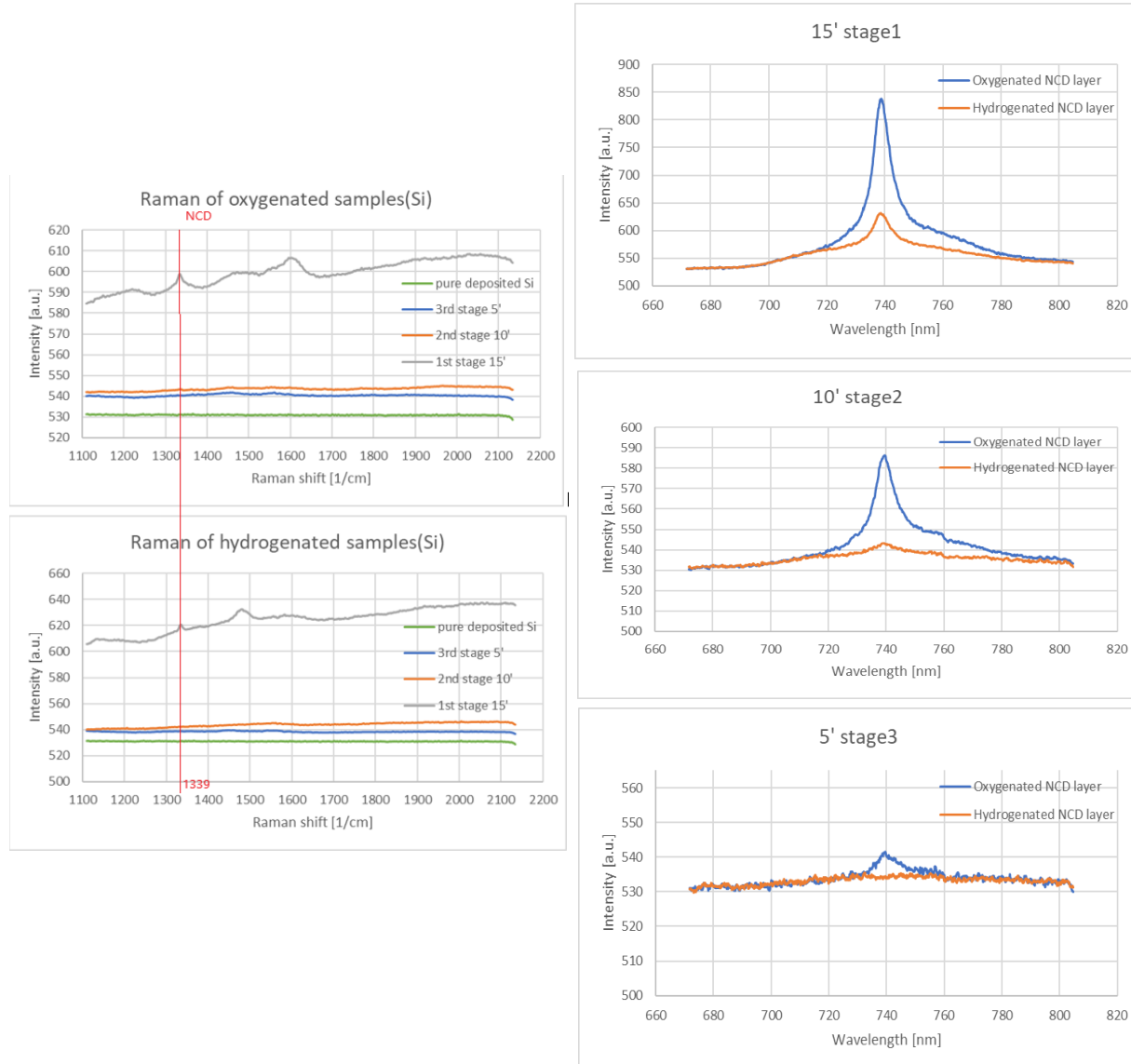


[Figure 5.1: On the left: Raman spectrum comparison with an NCD peak of O-term NCD(top) and H-term NCD(bottom) of NCD “fine” thin layer samples deposited for 5, 10 and 15 minutes and pure silicon, with NCD peak at 1339 cm⁻¹. On the right: PL of the NCD surface with an Si-V peak at 738 nm of thin layer samples deposited for 5(bottom), 10(middle) and 15 minutes(top) with O-term and H-term NCD comparison on each]

Si-V characteristic on the NCD surface is presented on the Figure 5.1 as well. Laser integration time is 300[s]. For thicker sample of 92[nm] or 15 minutes deposition we can see a larger NCD peak, than that of 10 (32 nm) and 5 (25 nm) minutes and O-term samples, the ones that were oxygen terminated, display higher Si-V properties, than H-term samples, with hydrogenated NCD layer Si-V peak not even visible for higher times (30 minutes).

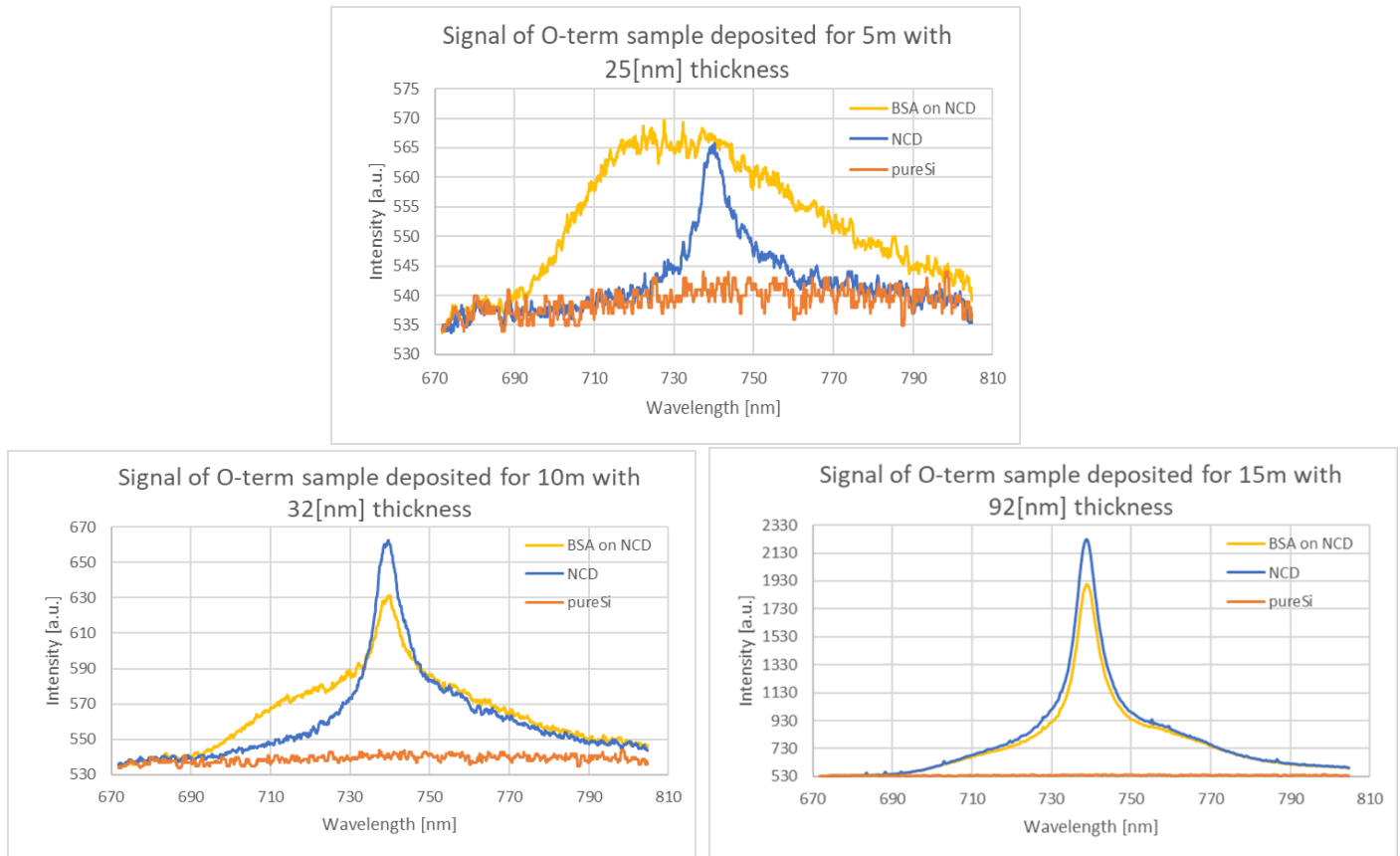


[Figure 5.2: PL spectrum of the drop-cast NCD samples of 25[nm], 32[nm] and 92[nm] with BSA on top (O-term)]

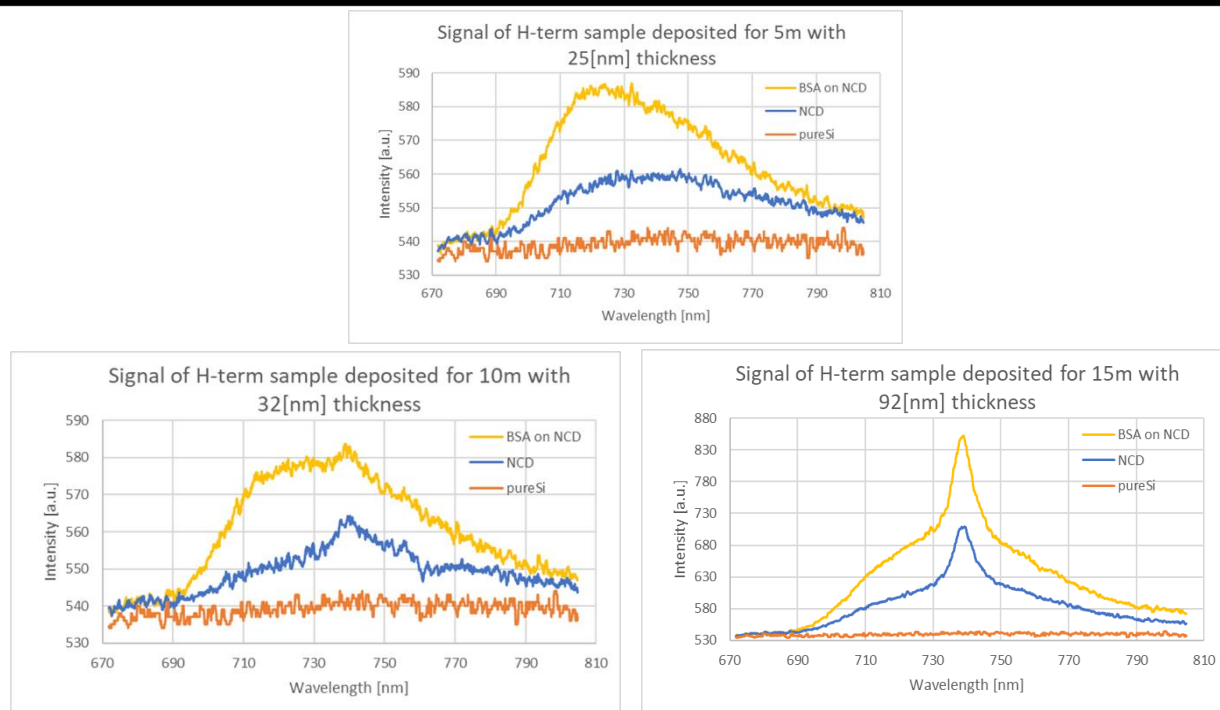


[Figure 5.3: PL spectrum of the drop-cast NCD samples of 25[nm], 32[nm] and 92[nm] with BSA on top (H-term)]

Furthermore, the 25[nm], 32[nm] and 92[nm] samples were drop-cast with BSA. The spectrum on Figure 5.2 shows the influence of BSA on Si-V peak. It seems that for thicker samples the influence has a structure of the Si-V peak itself, and as the NCD layer gets thinner, the BSA characteristic is shown as an influence, that does not resemble a peak, between the 710 and 770[nm]. According to the Figure 5.2, influence of BSA on Si-V peak is its stretching, but the same also happens in pure Si, which makes me believe that this is a pure BSA characteristic, and it mutes the Si-V peak in thinner samples completely. Same could be seen of Figure 5.3 and the Si-V peak intensity disappears and the BSA characteristic prevails. These measurements were done under the integration time of 5 minutes.

There could also be other possibilities, such as in thicker NCD layers, the protein reduces the Si-V signal. But at the same time, on Figure 5.3 for example, for H-term samples that were not put under oxygen plasma for 4 minutes under 100W, the Si-V peak is enhanced for the samples of all three thicknesses. For the 92[nm] NCD layer it is enhanced by almost 17% with a weird structure. Usually, a peak would look identical from both sides (e.g., Figure 5.1), but here BSA has a slightly elevated part from 710[nm] to ~730[nm], which I conceptualize to be the BSA characteristic mixed with an Si-V peak, as on the 32[nm] and 25[nm] samples of H-term and on the 32[nm] and 25[nm] of O-term samples we could see the same behavior. But we cannot see it on 92[nm] O-term, because the PL peak is too large, which is what we expected and why we created the thinner layer samples. As a result, the NCD Si-V surface could be influenced by the chemicals, and it appears to diminish the Si-V vacancy properties in the oxygen terminated NCD layer and enhance them in the hydrogenated NCD layers. Although, it could have been a singular incident and more observations are required.

This BSA characteristic seems to only appear on the NCD surface with an Si-V vacancy. For pure silicon the PL signal at 748[nm] and its range is non-existent, the spectrum is still. And when we drop-cast BSA on top of pure silicon it strangely had little to no effect(Figure 5.4).

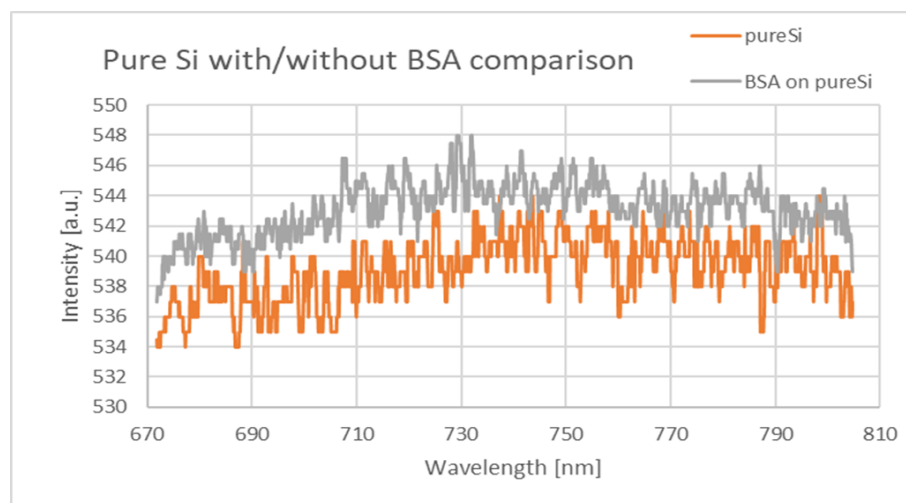


[Figure 5.4: PL spectra of pure silicon with two signals: from the Si surface and from BSA drop-cast on top of it]

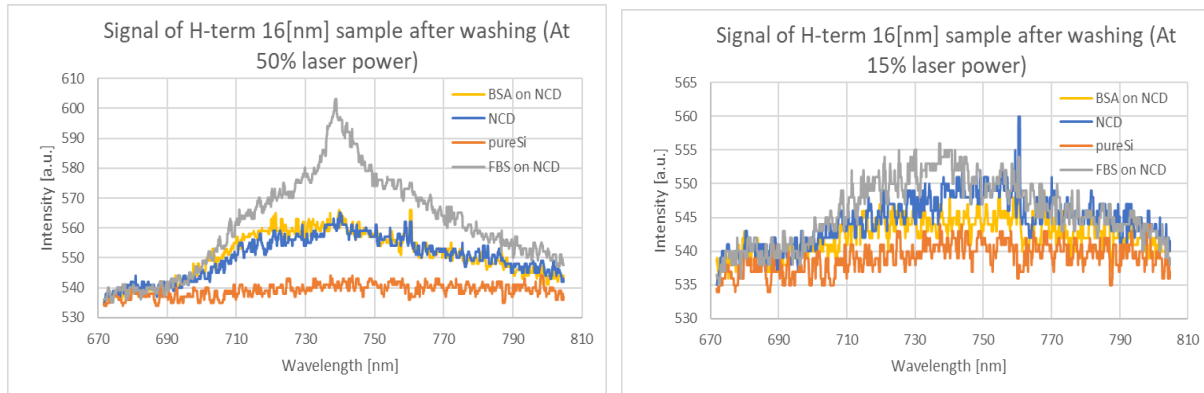


[Figure 5.5: PL spectra of 16[nm] thick “fine” NCD layer at 50% laser power(left) and 15% laser power(right) with signals of pure Si(orange); NCD(blue); washed BSA drop-cast on NCD(yellow) and washed FBS drop-cast on NCD(grey)]

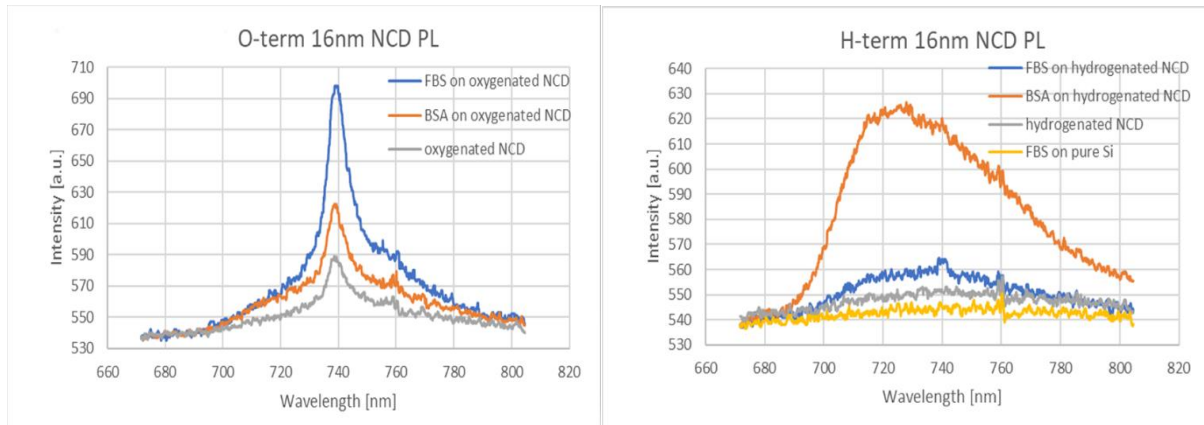


[Figure 5.6: PL spectra of 16[nm] thick “fine” H-term(right) and O-term(left) NCD layers with signals of FBS on pure Si(yellow); NCD(blue); BSA drop-cast on NCD(orange) and FBS drop-cast on NCD(blue)]

On the Figure 5.5 are two PL analysis spectrums of the same H-term ultrathin 16[nm] NCD “fine” sample. The only distinguishing factor is the laser power, which we increased from 15% or $\sim 4[\mu\text{W}]$ to 50% or $\sim 8[\mu\text{W}]$ and it seems that by increasing the laser power, FBS has some impact on the NCD layer. Si-V peak that is barely visible for NCD signal on the left spectra at 560[a.u.] is enhanced by the FBS to nearly 605[a.u.] of intensity. The signals of NCD and BSA have elevated as well, but do not display any apparent characteristics, so BSA was unaffected by the power increase.

Oxygen terminated NCD always displays a peak larger than of the hydrogenated NCD layer (from Figure 5.1). And the 16[nm] NCD layer samples are no different. But the interesting features arise here, as for the oxygen terminated sample of 16[nm], BSA and FBS enhance the Si-V peak, which seemingly contradicts the previous claim made according to the Figure 5.2 about BSA diminishing the Si-V characteristic in the oxygen terminated NCD layer. However, on the Figure, the BSA signal of 25[nm] displays a slightly larger intensity, even

though there is no Si-V peak at 738-739[nm]. From this data, a theory could be made, that the protein elevates the NCD characteristic defect under ultrathin thicknesses of ~25[nm] or less. Additionally, under the influence of FBS chemical the Si-V vacancy peak has increased in intensity two-three times as much as from the BSA influence. However, on the H-term 16[nm] NCD layer the opposite is experienced, as the BSA's intensity is much larger than that of hydrogenated NCD surface. The Si-V vacancy characteristic to NCD is not seen at 738-739[nm], because of the sample's hydrogenated nature. Moreover, a possible cause could be the weak laser power (~4 μ W), so the signal is not clear enough, which is also supported by the Figure 5.5.

Thickness of the proteins on top of the NCD surface from four regions, two in the middle and two on the edges was calculated to be 1.9[um] for BSA and 2.0[um] for FBS, so they are approximately of the same thickness. On BSA protein there was one scan of topography, that after measuring with the help of Gwyddion showed value much larger than presumed. The thickness ranged between 0.2[um] to 4[um] normally. The layer is more homogeneous in the middle than on the sides and it showed a value of 11[um], 2 times larger on 1 side than in the middle, which could be, but more likely that the AFM failed, because it was done on the scratched area(Si layer) and for Si layer it was showing height 1.8[um], which is impossible. For this reason, I do not count this measurement and thickness in calculation of the average thickness for this protein.

5.2 – Further extensibility and recommendations

As mentioned, the potential to biosensors in the optically active NCD surface with Si-V vacancies is present, but unclear part is its direct influence on the Si-V characteristic and the NCD surface. Higher laser power made an FBS, drop-cast on top of the NCD, impact the Si-V vacancy signal as presented on the Figure 5.5, so for further experiments, laser power of above 4~7[um] is insighted to be used.

More investigations regarding the chemical layer thickness as well as the concentration are required to understand the effect.

Bibliography

61

- [1] Christopher M. Breeding; Wuyi Wang. Diamond and Related Materials. "Occurrence of the Si-V defect center in natural colorless gem diamonds". (2008). Volume 17, issues 7-10, pages 1335 – 1344.
<https://reader.elsevier.com/reader/sd/pii/S0925963508001258?token=49E0E540084495999B322613BE677DC8FED44095F5A079C7A4451CCBF1803623046A8C0C3CF4A7556561C3316ADDAC73&originRegion=eu-west-1&originCreation=20220813232249>
- [2] Stepan Stehlik; Marian Varga; Pavla Stenclova; Lukas Ondric; Martin Ledinsky; Jiri Pangrac; Ondrej Vanek; Jan Lipov; Alexander Kromka; Bohuslav Rezek. Applied Materials & Interfaces. "Ultrathin Nanocrystalline Diamond Films with Silicon Vacancy Color Centers via Seeding by 2 nm Detonation Nanodiamond". (2017). Volume 9, pages 38842-38853
- [3] Wikipedia. Chemical Vapor Deposition journal; Chemical Vapor Deposition". (2021). paragraph 1
https://en.wikipedia.org/wiki/Chemical_vapor_deposition
- [4] Zhiping Ju, Junjie Lin, Si Shen, Butao Wu, E Wu. Advances in Physics. "Preparation and application of single-color centers in diamonds". (2021). Vol.6, no.1
<https://www.tandfonline.com/doi/epub/10.1080/23746149.2020.1858721?needAccess=true>
- [5] M. Veres, M. Koós, S. Tóth and L. Himics; Research Institute for Solid State Physics and Optics of the Hungarian Academy of Sciences, PO Box 49, H-1525 Budapest, Hungary. IOP Conf. Series: Materials Science and Engineering 15 (2010) 012023; "Sp₂ carbon defects in nanocrystalline diamond detected by Raman spectroscopy". (2010). doi:10.1088/1757-899X/15/1/012023. pages 1-7.
https://www.researchgate.net/publication/241470955_Sp2_carbon_defects_in_nanocrystalline_diamond_detected_by_Raman_spectroscopy
- [6] Fu-Lun Chen, Yu-Jui Fan, Jia-De Lin, and Yu-Cheng Hsiao. Biomedical optics express; "Label-free, color-indicating and sensitive biosensors of cholesteric liquid crystals on a single vertically aligned substrate". (2019). Vol.10, issue 19, pages 4636-4642.
<https://opg.optica.org/boe/fulltext.cfm?uri=boe-10-9-4636&id=416912>
- [7] PPG Quimica Descentes. Theory of sonochemistry; "The Ultrasonic Baths". (2022). chapter2; pages 49-61. https://www.academia.edu/33161948/The_ultrasonic_bath
- [8] Plasma Etch, Services Through Innovation. Home>Learn>Plasma Treatments>Oxygen Plasma Treatment. (2020). page 1. <https://www.plasmaetch.com/oxygen-plasma-treatment.php#:~:text=What%20is%20Oxygen%20Plasma%3F,such%20as%20plastic%20and%20rubber.>
- [9] Adamas Nan; Brilliant Diamond Solutions. "What is detonation nanodiamond?" (2022). page 1.
<https://www.adamasnano.com/what-is-detonation-nanodiamond/>
- [10] K D Vernon-Parry, Centre for electronic materials, UMIST. III-Vs Review: "Scanning electron microscopy, an introduction" (2000). Volume 13, issue 4, pages 40-44.
<https://reader.elsevier.com/reader/sd/pii/S096112900080006X?token=3C2C6D032AC36DAB9DF1BB91CF8F22DB98BDB98C69C5C5F160DC50949D38A0A1A16E65CE092921F83ABD0B1E5A0E9F27&originRegion=eu-west-1&originCreation=20220728194245>

- [11] Susan Swapp, University of Wyoming. "Scanning electron microscopy (SEM)". (2017) https://serc.carleton.edu/research_education/geochemsheets/techniques/SEM.html
- [12] Peter R. Schreiner. Quantum Mechanical Tunneling is Essential to Understanding Chemical Reactivity. (2020). Volume 2, Issue 11, pages 1 [https://www.cell.com/trends/chemistry/fulltext/S2589-5974\(20\)30215-X?_returnURL=https%3A%2F%2Flinkinghub.elsevier.com%2Fretrieve%2Fpii%2FS258959742030215X%3Fshowall%3Dtrue#articleInformation](https://www.cell.com/trends/chemistry/fulltext/S2589-5974(20)30215-X?_returnURL=https%3A%2F%2Flinkinghub.elsevier.com%2Fretrieve%2Fpii%2FS258959742030215X%3Fshowall%3Dtrue#articleInformation)
- [13] Jeol Ltd., 1-2 Musa Shino 3-chome Akishima, Tokyo 196-8558. SEM Scanning Electron Microscope from A to Z; "Basic knowledge for using the SEM". (2022). pages 1-31 https://www.jeol.co.jp/en/applications/pdf/sm/sem_atoz_all.pdf
- [14] JEOL. Top>Glossary of SEM>Stigmators. (2022). page 1. paragraph 1. https://www.jeol.co.jp/en/words/semterms/search_result.html?keyword=stigmator#:~:text=A%20stigmator%20is%20a%20device,through%20a%20set%20of%20coils.
- [15] Institute of Physics of the Czech Academy of Sciences. Characterization and Testing>Electron Microscopy. (2022). page 1 <https://www.fzu.cz/en/services/equipment-and-technologies/experimental-equipments/scanning-electron-microscope-maia-3>
- [16] TESCAN a.s., Brno, Czech Republic. Scanning Electron Microscope "MIRA3 FEG-SEM" Instructions for Use. (2011). pages 1-41 https://www.ccmr.cornell.edu/wp-content/uploads/sites/2/2019/01/MIRA_manual_GEN_3_04_tisk.pdf
- [17] Michael Schwander, Knut Partes. Diamonds & related materials, "A review of diamond synthesis by CVD processes". (2011). pages 1287 – 1301 <https://reader.elsevier.com/reader/sd/pii/S0925963511002913?token=6535183EF6A860FBAB15E3E7489E9BB0F06C405B43E33F3059D434A0E4F849730E122E8716DE65D36FBDD39164D76276&originRegion=eu-west-1&originCreation=20220805195703>
- [18] Wikipedia. "Chemical Vapor Deposition". (2021). paragraph 1-3. https://en.wikipedia.org/wiki/Chemical_vapor_deposition
- [19] V. Santhanam. Theory of Raman Spectroscopy. (2021). pages 1-29. <https://kanchiuniv.ac.in/coursematerials/Raman%20Spectra.pdf>
- [20] WI TEC focus innovations, Confocal Raman Microscopy, "Principles of confocal Raman Microscopy -> Introduction". (2021). page 1. paragraph 1.
- [21] Oxford instruments. «Introduction to Raman Spectroscopy Techniques». (2022). paragraphs 1-8. <https://andor.oxinst.com/learning/view/article/raman-spectroscopy>
- [22] Horiba Scientific. "Technologies -> Photoluminescence {PL} and Electroluminescence (EL)". (2022). paragraphs 1-6. <https://www.horiba.com/int/scientific/technologies/photoluminescence-pl/photoluminescence-pl-electroluminescence-el/>
- [23] Bob.Kyejune; African Institute of Mathematical Sciences. "Atomic Force Microscopy". (2022). pages 1-5. https://www.researchgate.net/publication/322294428_Atomic_Force_Microscopy

[24] Bruker. Products & solutions -> Microscopes -> AFM for materials -> Dimension Icon AFM. (2022). <https://www.bruker.com/en/products-and-solutions/microscopes/materials-afm/dimension-icon-afm.html>

[25] David Necas, Petr Klapetek. Gwyddion. Gwyddion>Home. (2021). paragraph 1-4. <http://gwyddion.net/>